UCLA
UCLA Previously Published Works

Title

Functional effects of disease-associated variants reveal that the S1-M1 linker of the NMDA receptor critically controls channel opening.

Permalink

https://escholarship.org/uc/item/5xt563b5

Journal

Cellular and Molecular Life Sciences, 80(4)

Authors

Xie, Lingling

McDaniel, Miranda

Perszyk, Riley

et al.

Publication Date

2023-03-31

DOI

10.1007/s00018-023-04705-y

Peer reviewed

Functional effects of disease-associated variants reveal that the S1–M1 linker of the NMDA receptor critically controls channel opening

Lingling Xie[1,13] · Miranda J. McDaniel[1] · Riley E. Perszyk[1] · Sukhan Kim[1,2] · Gerarda Cappuccio[3,14,15] · Kevin A. Shapiro[4] · Beatriz Muñoz-Cabello[5] · Pedro A. Sanchez-Lara[6] · Katheryn Grand[6] · Jing Zhang[1] · Kelsey A. Nocilla[1] · Rehan Sheikh[1] · Lluis Armengol[7] · Roberta Romano[3] · Tyler Mark Pierson[8,9,10,11] · Hongjie Yuan[1,2] · Scott J. Myers[1,2] · Stephen F. Traynelis[1,2,12]

Abstract

The short pre-M1 helix within the S1–M1 linker (also referred to as the pre-M1 linker) between the agonist-binding domain (ABD, S1) and the M1 transmembrane helix of the NMDA receptor (NMDAR) is devoid of missense variants within the healthy population but is a locus for de novo pathogenic variants associated with neurological disorders. Several de novo variants within this helix have been identified in patients presenting early in life with intellectual disability, developmental delay, and/or epilepsy. In this study, we evaluated functional properties for twenty variants within the pre-M1 linker in *GRIN1*, *GRIN2A*, and *GRIN2B* genes, including six novel missense variants. The effects of pre-M1 variants on agonist potency, sensitivity to endogenous allosteric modulators, response time course, channel open probability, and surface expression were assessed. Our data indicated that virtually all of the variants evaluated altered channel function, and multiple variants had profound functional consequences, which may contribute to the neurological conditions in the patients harboring the variants in this region. These data strongly suggest that the residues within the pre-M1 helix play a key role in channel gating and are highly intolerant to genetic variation.

Keywords Glutamate receptors · Channelopathy · *GRIN* · GluN · Pre-M1 · Translational study

✉ Stephen F. Traynelis
strayne@emory.edu

1 Department of Pharmacology and Chemical Biology, Emory University School of Medicine, 1510 Clifton Road, NE, Atlanta, GA 30322, USA

2 Center for Functional Evaluation of Rare Variants (CFERV), Emory University School of Medicine, Atlanta, GA 30322, USA

3 Present Address: Section of Pediatrics, Department of Translational Medicine, Federico II University, Via Pansini 5, 80131 Naples, Italy

4 Department of Neurology, University of California, UCSF Memory and Aging Center, Sandler Neurosciences Center, San Francisco, CA, USA

5 Department of Pediatrics, University Hospital Virgen del Rocío, Seville, Spain

6 Division of Medical Genetics, Department of Pediatrics, Cedars-Sinai Medical Center, Los Angeles, USA

7 Quantitative Genomic Medicine Laboratories, SL (qGenomics), Barcelona, Spain

8 Division of Pediatric Neurology, Department of Pediatrics, Cedars-Sinai Medical Center, Los Angeles, USA

9 Department of Neurology, Cedars-Sinai Medical Center, Los Angeles, USA

10 Center for the Undiagnosed Patient, Cedars-Sinai Medical Center, Los Angeles, USA

11 Board of Governors Regenerative Medicine Institute, Cedars-Sinai Medical Center, Los Angeles, USA

12 Emory Neurodegenerative Disease Center, Atlanta, GA 30322, USA

13 Present Address: Department of Neurology, Children's Hospital of Chongqing Medical University, Chongqing 400014, China

14 Present Address: Department of Pediatrics-Neurology, Baylor College of Medicine, Houston, TX, USA

15 Present Address: Jan and Dan Duncan Neurological Research Institute, Texas Children's Hospital, Houston, TX, USA

Abbreviations

3DMTR	Three-dimensional missense tolerance
7-CKA	7-chlorokynurenic acid
ABD	Agonist binding domain
AP-5	D,L-2-amino-5-phosphonovalerate
ASD	Autism spectrum disorder
ATD	Amino-terminal domain
CTD	Carboxyl-terminal domain
LBD	Ligand binding domain
MTSEA	2-aminoethyl methanethiosulfonate hydrobromide
NMDAR	*N*-methyl-D-aspartate receptor
NTD	N-terminal domain
TEVC	Two-electrode voltage clamp
TMD	Transmembrane domain (M1–4)
τ_W	Weighted deactivation tau
WT	Wildtype

Introduction

N-methyl-D-aspartate receptors (NMDARs) are ligand-gated ion channels that mediate a slow, Ca^{2+}-permeable component of excitatory synaptic transmission [1]. They are tetrameric assemblies of GluN1, GluN2A, GluN2B, GluN2C, GluN2D, GluN3A, and GluN3B subunits. Although the nature of potential triheteromeric receptors that contain GluN1, GluN2, and GluN3 subunits (GluN1/GluN2/GluN3) in native cells has been difficult to ascertain, receptors comprising other assemblies of these subunits are well characterized. Co-assembly of GluN1/GluN3 produces glycine-activated receptors, and classical NMDAR receptors arise from co-assembly of two GluN1 and two GluN2 subunits [1]. NMDARs are activated by the binding of both glutamate and glycine to the agonist binding domains (ABDs, also known as LBD, ligand binding domain) in the GluN2 and GluN1 subunits, respectively. Binding of both co-agonists to the NMDAR ABDs induces closure of the bilobed clamshell-like domains around the agonists, which triggers rearrangement of the linkers connecting the ABD to the ion channel pore and ultimately leads to opening of the pore [1]. Pore opening following agonist binding is controlled by multiple regions of the receptors, including the amino-terminal domain, linkers between domains, and membrane-associated portions (transmembrane domains M1–M4, TMD) of the receptor. Three closely spaced elements of the NMDAR within the transmembrane domain that control gating include the M3 transmembrane helix, the linker connecting the ABD to the M1 transmembrane helix (the pre-M1 linker or S1–M1 linker), and the linker preceding the M4 transmembrane helix of the adjacent subunit (the pre-M4 linker) [2]. The pre-M1 linker of all NMDAR subunits contains a two-turn helix (the pre-M1 helix) that lies parallel to the surface of the plasma membrane and has been proposed to control channel gating through van der Waals interactions with the pore-forming M3 transmembrane helix [2–8].

Use of the Genome Aggregation Database (gnomAD) to assess the variation in the *GRIN2A*/GluN2A and *GRIN2B*/GluN2B S1–M1 linker revealed a lack of missense variants between residues 540–555 for *GRIN2A* and 541–557 for *GRIN2B* in a population of over 140,000 healthy individuals (http://gnomad.broadinstitute.org, evaluated August 2022). A similar lack of variants was observed in *GRIN1*/GluN1 subunit in the pre-M1 linker (only 2 ultra-rare missense variants were reported in gnomAD between residues 545/566 in NP_015566). This lack of tolerated variation suggests that missense mutations in the pre-M1 linker could have significant effects on receptor function and, consequently, brain health. Evaluation of several missense variants residing in the GluN1 and GluN2A pre-M1 linker in patients with neurological conditions revealed significant functional consequences [9]. For example, GluN1-D552E and GluN1-P557R were identified in patients with intellectual disability and/or epilepsy, and both variants reduced current responses to saturating agonist and reduced surface expression relative to total expression when co-expressed with GluN2A [7]. These variants also altered glutamate and glycine potency. In addition, GluN2A-P552R identified in a patient with epilepsy slowed channel activation, prolonged the NMDAR deactivation time course, and markedly increased charge transfer [7]. A variant at the analogous residue, GluN2B-P553T, reduced channel function [10].

In this study, we have evaluated the functional properties of twenty additional pre-M1 variants identified in patients with neurological conditions to further explore the consequences of variation in this intolerant region. We expressed the GluN1, GluN2A, and GluN2B variants in heterologous systems and measured the effects on pharmacology, response time course, channel open probability, and receptor trafficking. We found multiple variants produced profound functional consequences, indicating that the residues within the pre-M1 linker, including the pre-M1 helix, play a critical role in channel function and may explain the neurological deficits identified in the patient with de novo missense variants in this region.

Materials and methods

Ethics, consent, study approval, and genetic analysis

This study was approved by the Medical Ethics Committee and the Institutional Review Boards of Federico II University (Italy), University of California, San Francisco (USA), University Hospital Virgen del Rocío (Spain), and Cedars-Sinai Medical Center (USA; Pr00037131).

Proband-1, -8, -9, -10, -14, -15, -18, and -24 (Supplemental Table S1) were registered and evaluated at Cedars-Sinai Medical Center (proband 1; GluN1- R548Q), University of California, San Francisco (probands 8, 9, 10; GluN2A-S545L), Federico II University (probands 14, 15, 24; GluN2A-S554T, GluN2B-S541G, and GluN2B-S555N), and University Hospital Virgen del Rocío (proband 18; GluN2B-A549V) by whole exome sequencing. All genomic DNA used in the experiments was extracted from peripheral leukocytes or buccal samples. All the variants were validated by Sanger sequencing.

All in vitro studies were conducted according to the guidelines of the Emory University Health and Safety Office and the Institutional Review Board.

Three-dimensional missense tolerance determination

The three-dimensional missense tolerance (3DMTR) [11] was determined for each of the diheteromeric NMDARs using homology models based on the non-active GluN1/GluN2B structure (pdb: 6WHS) [12] and the non-neuro gnomAD (v.2.1.1) dataset for each subunit. The 3DMTR application (https://github.com/riley-perszyk/3DMTR) was used to perform all analysis and score colored models, which were then used in PyMol to produce structure images.

Molecular biology

Human complementary DNAs (cDNAs) encoding human GluN1, GluN2A, and GluN2B were used as templates for site-directed mutagenesis with QuikChange Lightning Site-Directed Mutagenesis Kit (Agilent Technologies, Santa Clara, CA, USA) to replicate the parental cDNA strand with the desired mismatch incorporated into the oligonucleotide primer. Methylated parental cDNA was digested with Dpn I for 1 h at 37 °C and the nicked mutant cDNA was transformed into XL10-Gold Ultracompetent Cells (Agilent Technologies, Santa Clara, CA, USA). Mini-prep plasmid DNA was prepared from selected bacterial colonies grown in overnight cultures using the Qiaprep Spin Miniprep kit (Qiagen, Hilden, Germany) and the entire open reading frame of the glutamate receptor cDNA was verified using dideoxy DNA sequencing to verify the installation of the intended mutation and confirm no secondary site mutations were present (Eurofins Genomics, MWG Louisville, KY, USA). The human wildtype (WT) GluN1-1a (hereafter GluN1; NM_007327; NP_015566), human GluN2A (NM_000833; NP_000824) and human GluN2B (GenBank accession codes: NM_000834; NP_000825) cDNA were subcloned into the pCI neo vector [13].

The cDNA for WT and variant NMDAR subunits was linearized using FastDigest (Thermo Fisher, Waltham, MA, USA) restriction digestion at 37 °C for 1 h and the corresponding complementary RNA (cRNA) was synthesized in vitro using the mMessage mMachine T7 kit according to manufacturer's instructions (Invitrogen, Waltham, MA USA).

Unfertilized *Xenopus laevis* oocytes (stage V–VI) were prepared from commercially available ovaries (Xenopus One Inc, Dexter, MI, USA), which were digested with Collagenase Type 4 (Worthington-Biochem, Lakewood, NJ, USA) (800 µg/ml in dw, 15 ml for a half ovary) in Ca^{2+}-free Barth's solution, which contained (in mM) 88 NaCl, 2.4 $NaHCO_3$, 1 KCl, 0.82 $MgSO_4$, and 10 HEPES (pH 7.4 with NaOH), supplemented with 100 µg/ml gentamycin and 1 U/ml penicillin/streptomycin. The ovary was incubated in enzyme solution with gentle mixing at room temperature (RT, 23 °C) for 2 h. The oocytes were then rinsed 10 times with Ca^{2+}-free Barth's solution (35–40 ml of fresh solution each time) for 5 min each time and further rinsed 4 times with normal Barth's solution (same as above supplemented with 0.41 mM $CaCl_2$ and 0.33 mM $Ca(NO_3)_2$) on the slow shaker for 5 min each rinse. The oocytes were then kept in 16 °C incubator until further use. *Xenopus laevis* oocytes were injected with cRNA encoding either WT or mutant NMDAR subunits (GluN1:GluN2A or GluN2B ratio 1:2 for 5-10 ng total weight in 50 nl of RNAase-free water per oocyte). Injected oocytes were maintained in normal Barth's solution at 16 °C.

Two-electrode voltage-clamp current recordings from *Xenopus laevis* oocytes

Two-electrode voltage clamp (TEVC) current recordings were performed at room temperature (23 °C) as previously described [14–16]. A dual-stage micropipette puller (PC-10; Narishige, Japan) was used to prepare the electrodes from borosilicate glass (#TW150F-4; World Precision Instruments, Sarasota, FL, USA). Current and voltage electrodes were filled with 3 M KCl and used for TEVC recordings of oocytes one to five days postinjection (amplifier model OC-725C; Warner Instruments, Hamden, CT, USA). Oocytes were transferred to a dual-track recording chamber that shared a single perfusion line and allowed simultaneous recording from two oocytes. Oocytes were perfused with extracellular recording solution that contained (in mM) 90 NaCl, 1 KCl, 0.5 $BaCl_2$, 10 HEPES, and 0.01 EDTA (pH 7.4 with NaOH unless otherwise stated; no EDTA for experiments measuring Mg^{2+} or Zn^{2+} sensitivity). The extracellular recording solution was supplemented with 10 mM tricine for experiments evaluating Zn^{2+} sensitivity [17], and the following buffered free Zn^{2+} concentrations were achieved by adding

nominal concentrations of $ZnCl_2$ to tricine-containing external solution: for 1 nM free Zn^{2+} we added 0.14 µM $ZnCl_2$, for 3 nM free Zn^{2+} we added 0.42 µM $ZnCl_2$, for 10 nM free Zn^{2+} we added 1.4 µM $ZnCl_2$, for 30 nM free Zn^{2+} we added 4.2 µM $ZnCl_2$, for 100 nM free Zn^{2+} we added 14 µM $ZnCl_2$, for 300 nM free Zn^{2+} we added 42 µM $ZnCl_2$. Solution exchange was computer-controlled through an 8-valve positioner (Digital MVP Valve, Hamilton, CT, USA). Current responses to agonist application were recorded under a voltage clamp at a holding potential of -40 mV unless otherwise stated. All solutions for concentration–response experiments were made in the extracellular recording solution. Maximal concentrations of agonists (100 µM glutamate and 100 µM glycine) were used in all oocyte recordings unless otherwise stated. The covalent modifying reagent 2-aminoethyl methanethiolsulfonate hydrobromide (MTSEA; Toronto Research Chemicals, Ontario, Canada) was prepared fresh and used within 30 min.

Whole cell voltage clamp recordings

Human embryonic kidney (HEK) 293 cells (ATCC CRL-1573) were plated on glass coverslips pretreated with 0.1 mg/ml poly-D-lysine and cultured in Dulbecco's modified Eagle medium (DMEM) supplemented with 10% fetal bovine serum and 10 U/ml penicillin and 10 ug/ml streptomycin and maintained at 37℃ in a humidified environment with 5% CO_2. The cells were transiently transfected with cDNA encoding GluN1, GluN2A, and eGFP at a ratio of 1:1:5, or GluN1, GluN2B, and eGFP at a ratio of 1:1:3 by using the calcium phosphate precipitation method [15]. NMDAR antagonists (200 µM DL-APV and 200 µM 7-CKA) were added after the transfection. After 12–24 h following transfection, the cells were perfused with an external recording solution that contained (in mM) 3 KCl, 150 NaCl, 0.01 EDTA, 1.0 $CaCl_2$, 10 HEPES, and 22 D-mannitol (the pH was adjusted to 7.4 with NaOH). The patch electrodes (resistance 3–5 MΩ) were prepared from thin-walled glass micropipettes (TW150F-4, World Precision Instruments, Sarasota, FL, USA) by a dual-stage glass micropipette puller (PC-10, Narishige, Tokyo, Japan) and filled with an internal solution containing (in mM) 110 D-gluconate, 110 CsOH, 30 CsCl, 5 HEPES, 4 NaCl, 0.5 $CaCl_2$, 2 $MgCl_2$, 5 BAPTA, 2 NaATP and 0.3 NaGTP (pH was adjusted to 7.4 with CsOH; osmolality was adjusted to 300–305 mOsmol/kg).

The whole cell current responses were evoked by the application of maximally-effective concentrations of agonists (1 mM glutamate and 100 µM glycine) at a holding potential of -60 mV and recorded by an Axopatch 200B amplifier (Molecular Devices, Union City, CA, USA). All whole-cell recordings were performed at room temperature (23 ℃). The current responses were low pass filtered at 8 kHz with an 8-pole Bessel filter (− 3 dB; Frequency Devices) and digitized at 20 kHz using a Digidata 1440A acquisition system (Molecular Devices) controlled by Clampex 10.3 (Molecular Devices). The position of a two-barreled theta-glass micropipette used for rapid solution exchange was controlled by a piezoelectric translator (Burleigh Instruments, Newton, NJ, USA).

Beta-lactamase assay

HEK cells were plated in 96-well plates at a density of 50,000 cells/well. The cells were transiently transfected approximately 24 h later with cDNA encoding beta-lactamase (β-lac)-GluN1 variants with WT GluN2A, or β-lac-GluN2 variants with WT GluN1 using Fugene6 (Promega, Madison, WI). The β-lac-open reading frame was fused in the frame at the end of the signal peptide sequence for GluN1, GluN2A, or GluN2B receptors [18]. Several wells in each plate were treated with Fugene6 alone without cDNA to define background absorbance. Six wells were transfected for each condition to allow the determination of surface and total protein levels in three wells each. NMDAR antagonists (200 µM DL-APV and 200 µM 7-CKA) were added at the time of transfection. After 24 h, cells were rinsed with Hank's Balanced Salt Solution (HBSS) containing (in mM) 140 NaCl, 5 KCl, 0.3 Na_2HPO_4, 0.4 KH_2PO_4, 6 glucose, 4 $NaHCO_3$ and supplemented with 10 mM HEPES (pH 7.4). Subsequently, 100 µl of a 100 µM nitrocefin (Millipore, Burlington, MA, USA) solution in HBSS with HEPES was added to each of the three wells for measuring the level of extracellular enzymatic activity, which reflected surface expression of NMDAR. The cells in the other three wells were lysed by a 30 min incubation in 50 µl H_2O prior to the addition of 50 µl of 200 µM nitrocefin to determine the expression level of total enzymatic activity, which reflects the total NMDAR protein level. The absorbance at 486 nm was determined using a microplate reader every min for 30 min at 30 ℃. The rate of increase in absorbance was generated from the slope of a linear fit to the data.

Data and statistics analysis

Statistical analyses were performed in GraphPad Prism 8.0.1 (La Jolla, CA, USA) and OriginPro 9.0 (Northampton, MA, USA). Statistical significance was assessed using one-way ANOVA with post hoc Dunnett's multiple comparison test, with $p < 0.05$ considered significant. Data are presented as mean $\pm$ standard error of the mean (SEM). Error bars in

figures represent SEM unless otherwise stated. Power was determined using GPower 3.1.

EC_{50} values and IC_{50} values were obtained by fitting the concentration–response curve with Eqs. (1) and (2), respectively:

$$\text{Response}(\%) = 100/\left(1 + \left(EC_{50}/[\text{agonist}]\right)^{N}\right) \quad (1)$$

where N is the hill slope, EC_{50} is the concentration of the agonist that produces a half-maximal effect,

$$\text{Response}(\%) = (100 - \text{minimum}) \\ /\left(1 + \left([\text{inhibitor}]/IC_{50}\right)^{N}\right) + \text{minimum} \quad (2)$$

where IC_{50} is the concentration of the inhibitor that produces a half-maximal effect, and minimum is the amplitude of the residual response at a saturating concentration of the inhibitor.

The channel open probability (P_{OPEN}) was estimated from the fold potentiation observed in MTSEA using the following equation [19]:

$$P_{OPEN} = (\gamma_{MTSEA}/\gamma_{CONTROL}) \times (1/\text{Potentiation}) \quad (3)$$

where γ_{MTSEA} and $\gamma_{CONTROL}$ were the single channel chord conductance values estimated from GluN1/GluN2A receptors and fold Potentiation was defined as the ratio of current in the presence of MTSEA to current in the absence of MTSEA; $\gamma_{MTSEA}/\gamma_{CONTROL}$ was 0.67 [19].

The rise time for current responses recorded from HEK cells was determined as the time measured for the response amplitude to reach between 10 and 90% of the peak current. The current deactivation response time course following removal of glutamate was fitted using ChanneLab (Synaptosoft, Decatur, GA, USA) by:

$$\text{Response} = \text{Amplitude}_{FAST}\left(\exp\left(-\text{time}/\text{tau}_{FAST}\right)\right) \\ + \text{Amplitude}_{SLOW}\left(\exp\left(-\text{time}/\text{tau}_{SLOW}\right)\right) \quad (4)$$

The weighted deactivation tau (τ_{w}) was calculated by:

$$\tau_{w} = (\text{Amplitude}_{FAST}\tau_{FAST} + \text{Amplitude}_{SLOW}\tau_{SLOW}) \\ /\left(\text{Amplitude}_{FAST} + \text{Amplitude}_{SLOW}\right) \quad (5)$$

Charge transfer was estimated as the product of peak whole-cell current response amplitude and the weighted deactivation tau (τ_{w}) for responses to prolonged application of glutamate divided by the cell capacitance. We evaluated the relative fold-change in synaptic and non-synaptic charge transfer with the following equations, as previously described [18, 20]:

Relative charge transfer$_{\text{Synaptic}}$

$$= \tau_{wMUT}/\tau_{wWT} \times P_{MUT}/P_{WT} \\ \times \text{Surf}_{MUT}/\text{Surf}_{WT} \times R_{GLY} \\ \times R_{GLU, \text{Synaptic}} \times Mg_{MUT}/Mg_{WT} \quad (6)$$

Relative charge transfer$_{\text{Non-synaptic}}$

$$= P_{MUT}/P_{WT} \times \text{Surf}_{MUT}/\text{Surf}_{WT} \times R_{GLY} \\ \times R_{GLU, \text{Non-synaptic}} \times Mg_{MUT}/Mg_{WT} \quad (7)$$

where τ_{W} is the mean weighted deactivation time constant, P is the receptor open probability, Surf is surface protein level, Mg is the residual % response remaining by 1 mM Mg^{2+} at a holding potential of -60 mV, and R_{GLY} and R_{GLU} are relative response in a given agonist concentration calculated from Eq. (1). The concentration of glutamate used for synaptic charge transfer ($R_{GLU, \text{Synaptic}}$) was 1×10^{-3} M and for non-synaptic charge transfer ($R_{GLU, \text{Non-synaptic}}$ was 1×10^{-7} M. The concentration of glycine was 3×10^{-6} M.

Results

Clinical phenotypes associated with pre-M1 variants

This study includes twenty missense and insertion/deletion variants within the sequence coding pre-M1 linker and short pre-M1 helix in the NMDAR *GRIN1*, *GRIN2A*, and *GRIN2B* genes. The variants studied here were absent from the gnomAD database (evaluated August 2022). Table 1 and Supplemental Table S1 summarize the clinical phenotype, the DNA and protein alteration, pathogenicity prediction, and source for each of these variants. These include six *GRIN1* variants, five *GRIN2A* variants, and nine *GRIN2B* variants. Five variants are novel (Patients-7,8,9, GluN2A-S545L; Patient-14, GluN2A-S554T; Patient-15, GluN2B-S541G; Patient-18, GluN2B-A549V; and Patient-24, GluN2B-S555N), while fifteen were reported in the academic literatures [10, 21–32] or ClinVar (Supplemental Table S1, Table 1) with one recurrent variant reported in this study (Patient-1, GluN1-R548Q). All 24 patients (Supplemental Table S1) presented with neurodevelopmental disorders (i.e., intellectual disability or developmental delay). In addition, eight of the patients presented with seizures (Supplemental Figure S1). Eleven patients had abnormal tone (hypotonia and/or hypertonia). Nine patients presented with speech and language problems. Among them, a father (Patient-10, 38-year-old), daughter (Patient-9, 11-year-old) and son (Patient-8, 9-year-old) were all symptomatic as a result

Table 1 Information of pre-M1 variants and patients' phenotypes

#	Variant	Gene	Genotype	Amino acid changes	Phenotype	Source
1	GluN1- R548Q	*GRIN1*	c.1643G>A	p.Arg548Gln	Epi, DD, ID, MD, ASD	This study, ClinVar, [31]
2	GluN1-S549R	*GRIN1*	c.1645A>C	p.Ser549Arg	Inborn genetic diseases, Epi, ID	ClinVar, [24, 25]
3	GluN1-L551P	*GRIN1*	c.1652T>C	p.Leu551Pro	Epi, ID, MD	[27, 30]
4	GluN1-P557L	*GRIN1*	c.1670C>T	p.Pro557Leu	ID, DD, LD, MD	ClinVar, [23]
5	GluN1-Q559R	*GRIN1*	c.1676A>G	p.Gln559Arg	ID, DD, MD	[29]
6	GluN1-S560insS	*GRIN1*	c.1679_1681dupGCA	p.Ser560insSer	Epi, ID	[21]
7	GluN2A-S545L	*GRIN2A*	c.1643C>T	p.Ser545Leu	Speech and language problems, abnormal EEG	This study
8	GluN2A-S547del	*GRIN2A*	c.1639_1641delTCT	p.Ser547del	ID, Epi, MD, LD	[22]
9	GluN2A-A548P	*GRIN2A*	c.1642G>C	p.Ala548Pro	Landau-Kleffner syndrome	ClinVar
10	GluN2A-E551K	*GRIN2A*	c.1651G>A	p.Glu551Lys	Inborn genetic diseases	ClinVar
11	GluN2A-S554T	*GRIN2A*	c.1661G>C	p.Ser554Thr	DD, ID, LD	This study
12	GluN2B-S541G	*GRIN2B*	c.1621A>C	p.Ser541Gly	Epi, DD, ID, MD, ASD	This study
13	GluN2B-S541R	*GRIN2B*	c.1623C>G	p.Ser541Arg	Epi, ID, MD, ASD	ClinVar, [28]
14	GluN2B-G543R	*GRIN2B*	c.1627G>C	p.Gly543Arg	Complex neurodevelopmental disorder, MD	ClinVar
15	GluN2B-A549V	*GRIN2B*	c.1646C>T	p.Ala549Val	Severe encephalopathy, DD, hypotonia	This study
16	GluN2B-F550S	*GRIN2B*	c.1649T>C	p.Phe550Ser	Inborn genetic diseases	ClinVar
17	GluN2B-L551S	*GRIN2B*	c.1652T>C	p.Leu551Ser	ID	[32]
18	GluN2B-P553T	*GRIN2B*	c.1657C>A	p.Pro553Thr	DD, Rett-like syndrome, Epi	[10, 26]
19	GluN2B-S555I	*GRIN2B*	c.1664G>T	p.Ser555Ile	Complex neurodevelopmental disorder, ID	ClinVar, [28]
20	GluN2B-S555N	*GRIN2B*	c.1664G>A	p.Ser555Asn	Epi, DEE, DD, ID, ASD	This study

ASD autism spectrum disorder, *DD* developmental delay, *Epi* epilepsy/seizures, *ID* intellectual disability, *LD* language disorder (including language delay, speech disorders), *MD* movement disorders

of a common mutation in *GRIN2A*_p.Ser545Leu (Supplemental Fig. S1). The daughter had a very abnormal EEG with ESES-like features at 5 years of age, although the spikes are not sleep-activated and normal sleep architecture was present. She has never had a clinical seizure, but her language, attention, and memory have responded well to a trial of Depakote (valproic acid). The son had speech-language delay and more modest abnormalities on EEG at 2-year-old. Father has never had an EEG or seizures but has a lifelong history of speech problems.

The affected residues within the pre-M1 region were present in GluN1, GluN2A, and GluN2B subunits, encoded by *GRIN1*, *GRIN2A*, and *GRIN2B* genes, respectively (Fig. 1). Tolerance to variation for genes encoding NMDA receptor subunit was assessed from the frequency of variants present in gnomAD, using the 3-dimensional structure to assess likelihood that a region is devoid of variants [11]. This analysis reveals strong sensitivity to variation of the linker and associated short helix that precedes the M1 transmembrane domain (Fig. 2, Supplemental Fig. S2, S3). Previous studies have shown intolerance in this region as well as functional consequences of human variants in the pre-M1 linker (e.g., [7, 10]). We introduced each of these variants into

cDNA encoding human GluN1, GluN2A, and GluN2B, and expressed these mutant cDNAs in heterologous systems that allowed us to assess the in vitro functional consequences of these variants.

Effects of pre-M1 variants on agonist potency

Two electrode voltage clamp recordings were performed on *Xenopus* oocytes co-injected with WT or variant GluN1 and WT GluN2A or GluN2B cRNA. Oocytes were held at −40 mV and current responses to the application of glutamate and glycine were recorded to evaluate the functional effects of these pre-M1 variants. Concentration–response curves were generated for the endogenous NMDAR agonists glutamate or glycine to determine their EC_{50} values and assess variant effects on agonist potency. We identified three GluN1 variants with confidence intervals for both glutamate and glycine EC_{50} values that were non-overlapping with wild-type NMDAR values. GluN1-R548Q co-expressed with GluN2A or GluN2B had a 3.3-fold and 1.9-fold lower glutamate EC_{50} than WT NMDARs, respectively, in the presence of maximally effective glycine (Fig. 3a, b, *upper panels*; Table 2). GluN1-R548Q
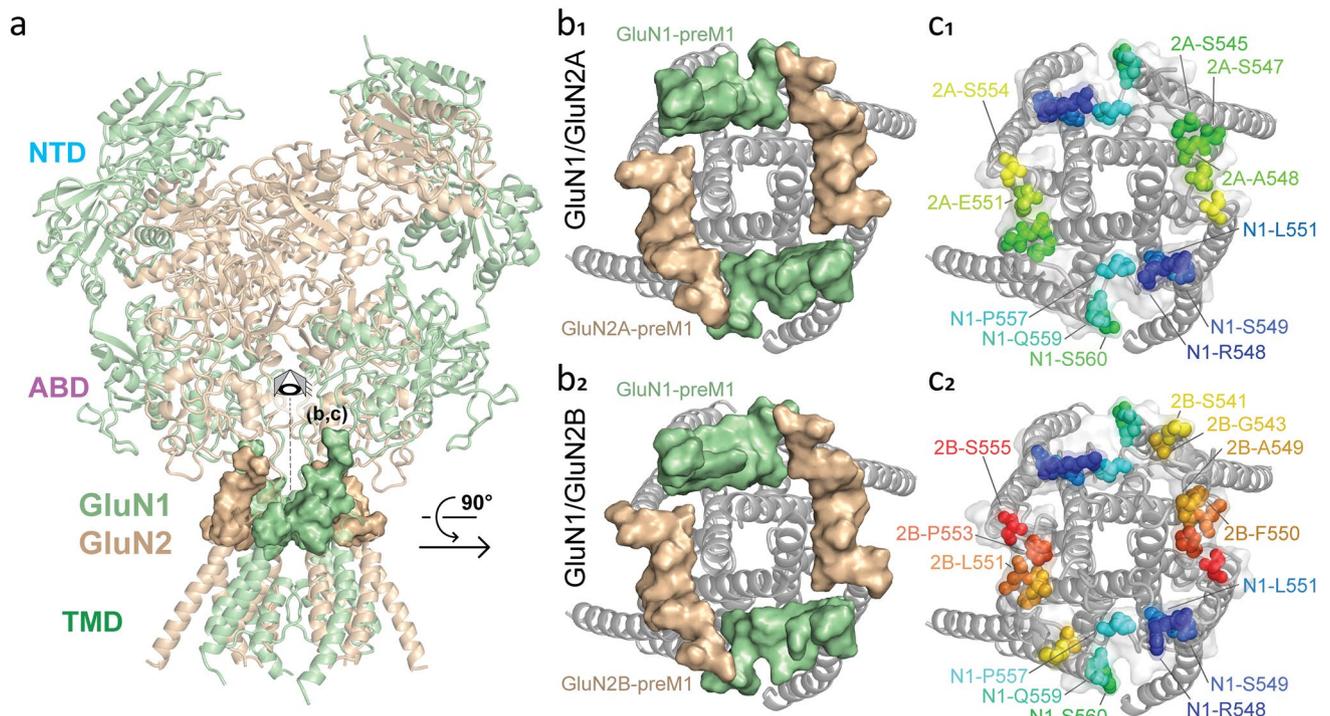
Fig. 1 Location of the affected residues in pre-M1 helix. **a** Structure of the GluN1/GluN2A homology model [11] shown as a ribbon structure overlaid with the pre-M1 domains shown in space-filling representation. GluN1 is in green, and GluN2 is in wheat. **b** The top-down view (depicted in **a**) of the pre-M1 linker and transmembrane domain of GluN1/GluN2A (**b1**) and GluN1/GluN2B (**b2**) [11]. **c** Sphere representation of the identified pre-M1 variants presented in this study. GluN1 variants are shown in both **c1** and **c2**, GluN2A variants is shown in **c1**, and GluN2B variants are shown in **c2**. NTD, N-terminal domain (also known as ATD, amino-terminal domain), ABD, agonist binding domain, TMD, transmembrane domain (three transmembrane helices M1, M3, M4 and a reentrant pore-forming loop M2)

co-expressed with GluN2A or GluN2B similarly had a 1.8-fold or 4.5-fold lower glycine EC_{50} in the presence of maximally effective glutamate than WT NMDARs, respectively (Fig. 3a, b, *lower panels*; Table 2). In addition, GluN1-L551P co-expressed with GluN2A or GluN2B had a 20-fold or 57-fold lower glutamate EC_{50}, and a 109-fold or 14-fold lower glycine EC_{50}, respectively, than WT NMDARs (Fig. 3a, b; Table 2). GluN1-S549R co-expressed with GluN2A possessed a 1.9-fold higher glutamate EC_{50} and a 2.5-fold higher glycine EC_{50} than observed for WT receptors. However, GluN1-S549R/ GluN2B currents were too small to measure. These data suggest variants in this region alter co-agonist potency and, in some cases, overall response amplitudes. We also observed that GluN1-Q559R co-expressed with GluN2A had a modest effect on glutamate potency with non-overlapping confidence intervals when compared to WT NMDARs. GluN1-P557L and GluN1-S560*ins*S did not produce currents large enough to accurately determine the EC_{50} value when co-expressed with either GluN2A or GluN2B.

We also performed two-electrode voltage clamp recordings on *Xenopus* oocytes co-injected with WT GluN1 and WT or variant GluN2A or GluN2B cRNA. NMDARs composed of GluN1 and GluN2A-E551K or GluN2A-S554T had statistically significant 6.7- and 4.6-fold decreases in glutamate EC_{50} compared to WT receptors (Fig. 3c, *upper panel*; Table 2), and showed 4.6-fold and 5.2-fold decreases in glycine EC_{50}, respectively (Fig. 3c, *lower panel*; Table 2). GluN2A-S545L modestly reduced glutamate and glycine potency compared to WT receptors (Fig. 3c; Table 2). Several GluN2A variants did not produce currents large enough to accurately determine EC_{50} values, including GluN2A-S547*del* and GluN2A-A548P.

GluN2B-S541G, GluN2B-G543R, GluN2B-S555N showed 4.3-, 5.9-, and 3.6-fold decreases in glutamate EC_{50} and similar 4.8-, 3.6-, and 2.8-fold decreases in glycine EC_{50}, respectively, compared to WT NMDARs (Fig. 3d; Table 2). By contrast, GluN2B-S541R and GluN2B-P553T decreased agonist potency, with glutamate EC_{50} increased by 7- and 1.9-fold, and glycine EC_{50} increased by 2.9- and
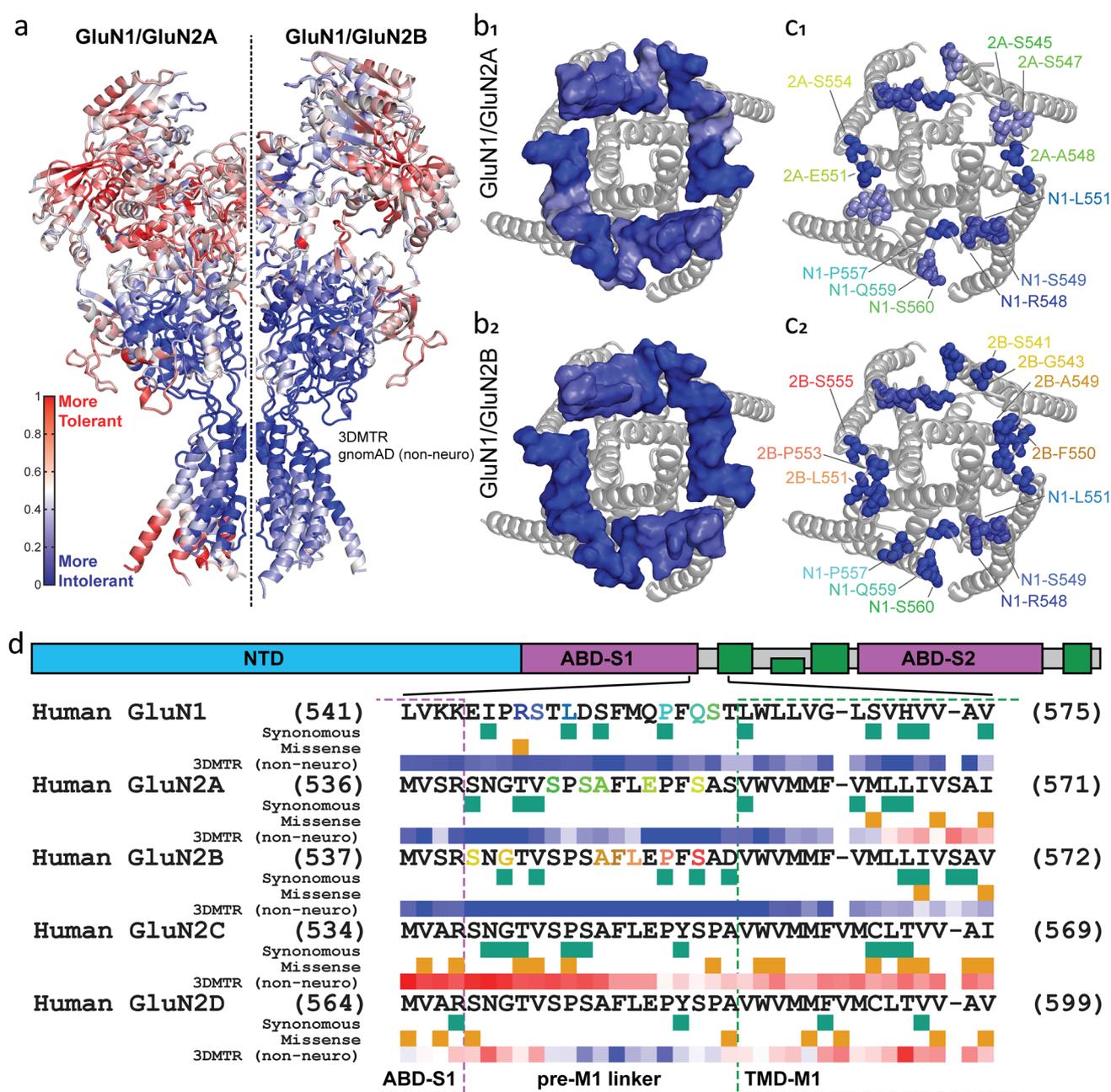
Fig. 2 The GluN1, GluN2A, and GluN2B pre-M1 linker is intolerant to genetic variation. **a** The 3DMTR score is shown represented as a heat map on the GluN1/GluN2A and GluN1/GluN2B structures. More tolerant scores are depicted by red shades and more intolerant score are depicted by blue shades (scale shown in the bottom left corner). The closest 31 residues were used in the intra-receptor calculation of the 3DMTR using the non-neuro gnomAD dataset (version 2.1.1). The heat map for each isolated subunit was presented in Supplemental Fig-S3. **b** The 3DMTR scores for the GluN1 (**b1** and **b2**), GluN2A (**b1**), and GluN2B (**b2**) pre-M1 linker residues are shown using the same view as in Fig. 1**b**. **c** The 3DMTR scores for the GluN1 (**c1** and **c2**), GluN2A (**c1**), and GluN2B (**c2**) pre-M1 variants are shown using the same top-down view as in Fig. 1**c**. **d** Linear domain representation of a GluN1 or GluN2 subunit and an alignment of the GluN1 and GluN2 pre-M1 sequences. Under each sequence, the residues that possess missense (gold) and synonymous (green) variants in gnomAD (non-neuro, version 2.1.1) are shown along with each residue's 3DMTR score represented as a heat map

3.2-fold compared to WT receptors (Fig. 3d; Table 2). Four GluN2B pre-M1 linker variants did not produce current responses large enough to accurately determine the agonist EC_{50} values, including GluN2B-A549V, GluN2B-F550S, GluN2B-L551S, GluN2B-S555I. These data together confirm that 90% of these variants produce detectable changes in agonist potency.
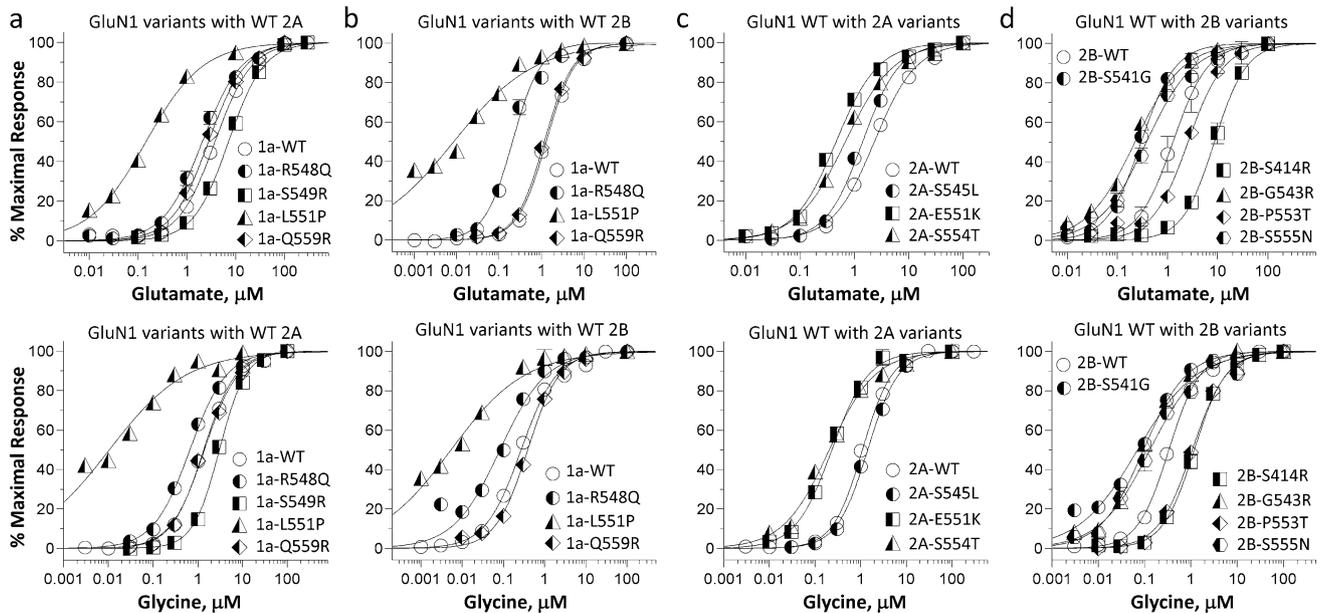
Fig. 3 Effects of pre-M1 transmembrane linker variants on NMDAR agonist potency. **a–d** Composite concentration–response curves for glutamate (*top panels*, in the presence of 100 μM glycine) and glycine (*lower panels*, in the presence of 100 μM glutamate) activation of WT and variant GluN1 co-expressed with GluN2A (**a**) or GluN2B (**b**), respectively, and WT GluN1 co-expressed with WT or variant GluN2A (**c**), and GluN2B (**d**). The curves were obtained from two-electrode voltage clamp recordings from oocytes at a holding potential of −40 mV

Effect of pre-M1 variants on sensitivity to negative allosteric modulators

One of the most important features of NMDARs is the negative regulation by endogenous extracellular allosteric modulators such as extracellular Mg^{2+}, Zn^{2+}, as well as protons. We evaluated the effect of extracellular Mg^{2+} by recording the current responses evoked by 100 μM glutamate and 100 μM glycine with different concentrations of Mg^{2+} at a holding potential of −60 mV. Two variant NMDARs showed increased sensitivity to Mg^{2+} channel block including GluN1-L551P/GluN2B and GluN1/GluN2B-S541R, whereas one variant (GluN2A-S554T) reduced Mg^{2+} block. These data suggest that most pre-M1 variants do not alter the sensitivity to extracellular Mg^{2+}, and those that do have relatively modest effects, although these may be meaningful in the context of physiological function (Fig. 4a, b; Table 2). This is consistent with the location of the pre-M1 linker, which is distant from the Mg^{2+} binding site deep within the pore. We also determined the effect of extracellular Zn^{2+} on the high-affinity binding site within the amino-terminal domain of the GluN2A subunit by recording the current responses from GluN1/GluN2A NMDARs evoked by 50 μM glutamate and 50 μM glycine with different concentrations of tricine-buffered Zn^{2+} at a holding potential of −20 mV, to minimize potential voltage-dependent channel block by higher concentrations of Zn^{2+}. The only variant

to show a detectable potency change was GluN1/GluN2A-S554T, which was 2.6-fold less sensitive to extracellular Zn^{2+} (Fig. 4c; Table 2).

NMDA receptors can be inhibited by extracellular pH with a nearly monotonic inhibition curve possessing an IC_{50} value near physiological pH, suggesting receptors are under tonic proton inhibition. The sensitivity to extracellular protons was evaluated by comparing the current amplitude recorded at two pH values pH 6.8 and pH 7.6 that bracket physiological pH. Measurements were made at a holding potential of −40 mV. All GluN1 variants showed altered current at pH 6.8 relative to pH 7.6 compared to WT NMDARs (Fig. 4d; Table 2). Similarly, most GluN2A and GluN2B variants also showed altered levels of proton inhibition (Fig. 4e; Table 2). For example, GluN1/GluN2A-E551K and GluN1/GluN2A-S554T, GluN1/GluN2B-S541R, GluN1/GluN2B- GluN2B-S555N showed modestly reduced inhibition at pH 6.8, which would reduce tonic inhibition at physiological pH and suggest enhanced current responses. GluN2B-P553T showed modestly enhanced levels proton inhibition.

Effects of pre-M1 variants on response time course and channel open probability

To determine whether the pre-M1 variants alter the overall response of NMDARs to agonist, we expressed WT

Table 2 Pharmacological properties of pre-M1 variants in NMDAR subunits

	Glutamate EC_{50} μM (95%CI) (n)	Glycine EC_{50} μM (95%CI) (n)	Mg^{2+} IC_{50} μM (95%CI) (n)	Zn^{2+} IC_{50} μM (95%CI) (n)	%, $pH_{6.8}$/$pH_{7.6}$ mean ± SEM (n)
WT 1a/2A	3.6 (3.3, 4.0) (47)	1.2 (1.1, 1.4) (43)	22 (19, 25) (45)	8.0 (6.8, 9.3) (48)	49 ± 1.3 (56)
1a-R548Q/2A	1.1 (0.92, 1.4) (14)*	0.66 (0.54, 0.81) (12)*	28 (22, 36) (13)	10 (6, 15) (12)	61 ± 2.2 (13)*
1a-S549R/2A	7.0 (5.6, 8.6) (17)*	3.0 (2.5, 3.5) (14)*	24 (18, 33) (13)	4.6 (3.1, 6.8) (12)	26 ± 3.9 (13)*
1a-L551P/2A	0.18 (0.15, 0.21) (12)*	0.011 (0.0076, 0.017) (13)*	20 (14, 29) (21)	8.0 (5.4, 12) (17)	26 ± 1.5 (19)*
1a-P557L/2A	ND	ND	ND	ND	ND
1a-Q559R/2A	2.8 (2.5, 3.1) (13)*	1.4 (1.2, 1.7) (15)	23 (19, 29) (11)	11 (8.4, 15) (12)	73 ± 1.1 (11)*
1a-S560insS/2A	ND	ND	ND	ND	ND
WT 1a/2B	1.3 (1.2, 1.4) (40)	0.37 (0.33, 0.43) (32)	27 (21, 33) (30)	NA	16 ± 0.93 (30)
1a-R548Q/2B	0.67 (0.53, 0.85) (12)*	0.083 (0.066, 0.10) (12)*	29 (21, 41) (9)	NA	26 ± 3.2 (9)[#]
1a-S549R/2B	ND	ND	ND	NA	ND
1a-L551P/2B	0.023 (0.018, 0.031) (11)*	0.026 (0.019, 0.037) (12)*	15 (13, 17) (12)*	NA	8.4 ± 1.2 (12)[#]
1a-P557L/2B	ND	ND	ND	NA	ND
1a-Q559R/2B	1.2 (0.91, 1.5) (12)	0.38 (0.28, 0.51) (14)	23 (17, 30) (12)	NA	28 ± 1.7 (12)[#]
1a-S560insS/2B	ND	ND	ND	NA	ND
WT 1a/2A	3.1 (2.8, 3.4) (32)	1.1 (1.0, 1.2) (39)	21 (18, 24) (35)	6.8 (6.2, 7.5) (38)	43 ± 1.2 (34)
2A-S545L	4.9 (4.5, 5.4) (11)*	1.4 (1.3, 1.6) (12)*	17 (14, 19) (12)	6.2 (4.9, 7.9) (12)	49 ± 2.2 (11)
2A-S547del	ND	ND	ND	ND	ND
2A-A548P	ND	ND	ND	ND	ND
2A-E551K	0.46 (0.41, 0.52) (12)*[a]	0.24 (0.19, 0.29) (12)*	18 (15, 23) (12)	7.8 (6.0, 10) (12)	52 ± 3.0 (12)[#]
2A-S554T	0.68 (0.55, 0.85) (12)*	0.21 (0.17, 0.26) (13)*	33 (26, 42) (11)*	18 (9.0, 34) (9)*	75 ± 1.2 (12)[#]
WT 1a/2B	1.3 (1.2, 1.4) (68)	0.34 (0.31, 0.37) (68)	27 (23, 32) (57)	NA	15 ± 0.44 (82)
2B-S541G	0.30 (0.24, 0.38) (11)*	0.071 (0.053, 0.095) (14)*	30 (20, 44) (12)	NA	18 ± 1.3 (11)
2B-S541R	9.1 (7.2, 11) (16)*	1.0 (0.71, 1.4) (17)*	18 (15, 22) (12)*	NA	18 ± 0.70 (19)[#]
2B-G543R	0.22 (0.19, 0.26) (15)*[a]	0.094 (0.077, 0.12) (15)*	26 (22, 31) (12)	NA	14 ± 1.5 (12)
2B-A549V	ND	ND	ND	NA	ND
2B-F550S	ND	ND	ND	NA	ND
2B-L551S	ND	ND	29 (23, 37) (5)	NA	ND
2B-P553T	2.5 (1.9, 3.3) (11)*	1.1 (0.89, 1.3) (14)*	25 (20, 30) (12)	NA	10 ± 0.78 (15)[#]
2B-S555I	ND	ND	ND	NA	ND
2B-S555N	0.36 (0.24, 0.56) (12)*	0.12 (0.073, 0.20) (12)*	40 (24, 67) (12)	NA	20 ± 1.4 (12)[#]

The glutamate concentration–response relationship was determined in the presence of 0.1 mM glycine, and the glycine concentration–response relationship were determined in the presence of 0.1 mM glutamate. Wild-type IC_{50}/EC_{50} values were from experiments performed the same day. Data shown are the mean IC_{50}/EC_{50} value with 95% confidence intervals determined from the $LogEC_{50}$ or $LogIC_{50}$ values. * indicates 95% confidence intervals that are non-overlapping with WT GluN2A- or GluN2B-containing NMDARs. Data are mean ± SEM for current ratio at different pH values, which were assessed by one-way ANOVA with post hoc Dunnett's multiple comparison test ([#]$p < 0.05$); n is the number of cells recorded from. ND indicates not determined due to low current amplitude. NA indicates not applicable as GluN2B does not harbor a high-affinity Zn^{2+} binding site

[a]Data are from Han et al. [52]

and variant NMDAR subunits in HEK cells and performed whole-cell voltage clamp recordings to determine whether there were changes in the response time course. We rapidly applied maximally active concentrations of glutamate (1000 μM) and glycine (100 μM) to HEK cells that had been lifted from the coverslip and placed into the flow stream, which allowed rapid piezo-driven solution exchange (see "Materials and methods"). We applied glutamate and glycine for either 1.5 s (prolonged; Fig. 5a, b, *left panels*) or 10 ms (brief; Fig. 5a, b, *right panels*), and measured the 10–90% rise time, the peak currents, and the time course of deactivation upon rapid removal of agonists to mimic synaptic events. Deactivation time courses were fitted by either a single or double exponential function and the weighted tau calculated as an overall indicator of whether the variant accelerated or slowed the deactivation time course. Table 3
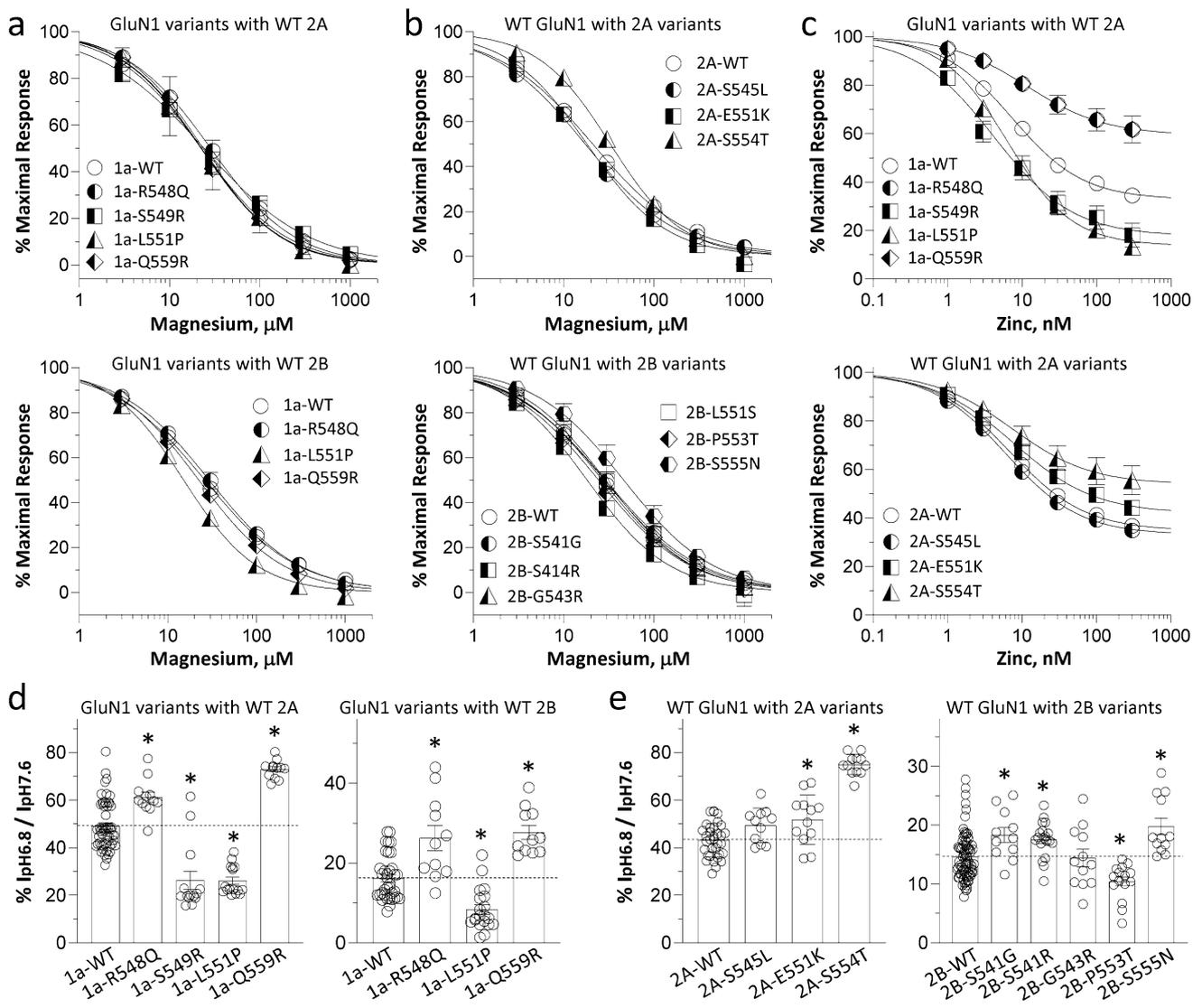
Fig. 4 Effects of pre-M1 transmembrane linker variants on sensitivity to NMDAR endogenous modulators. **a**, **b** Composite concentration–response curves for voltage-dependent Mg^{2+} block of the channel in the presence of 100 μM glutamate and 100 μM glycine at a holding potential of −60 mV for the GluN1 variants co-expressed with GluN2A (**a**, *top panel*) or GluN2B (**a**, *lower panel*), respectively, and GluN1 coexpressed with GluN2A variants (**b**, *top panel*) and GluN2B variants (**b**, *lower panel*). **c** Composite concentration–response curves for buffered Zn^{2+} on WT and variant GluN1/GluN2A

NMDARs. Smooth lines are fitted curves (*see* Materialsf and methods). **d**, **e** Summary of proton sensitivity evaluated by current ratio at pH 6.8 to pH 7.6 (in the presence of 100 μM glutamate and 100 μM glycine) at a holding potential of -40 mV for the GluN1 variants coexpressed with GluN2A (**d**, *left panel*) or GluN2B (**d**, *right panel*), respectively, and WT GluN1 coexpressed with GluN2A variants (**e**, *left panel*), and GluN2B variants (**e**, *right panel*). *$p < 0.05$, one-way ANOVA with Dunnett's multiple comparisons test, compared to WT

summarizes the weighted time constant describing the deactivation time course for each variant (see Supplemental Table S2 for individual fast and slow time constants). We found that several variant NMDARs have a significantly prolonged deactivation time course compared to WT, including GluN1-R548Q/GluN2A, GluN1-L551P/GluN2A, GluN1/GluN2A-E551K, GluN1/GluN2A-S554T, GluN1/GluN2B-S541G, and GluN1/GluN2B-S555N (Fig. 5c, d; Table 3). However, GluN1/GluN2B-S541R, GluN1/GluN2B-L551S,

and GluN1/GluN2B-P553T showed a significantly accelerated deactivation time course compared to WT (Fig. 5c, d; Table 3). GluN1-P557L, GluN1-S560insS, GluN2A-S547del, GluN2A-A548P, GluN2B-A549V, GluN2B-F550S, and GluN2B-S555I produced currents too small to reliably measure when expressed in HEK cells. In addition, we averaged the response amplitude from patch clamp whole-cell recordings in the experiments used to assess time course. Table 3 summarizes the results of this analysis and shows
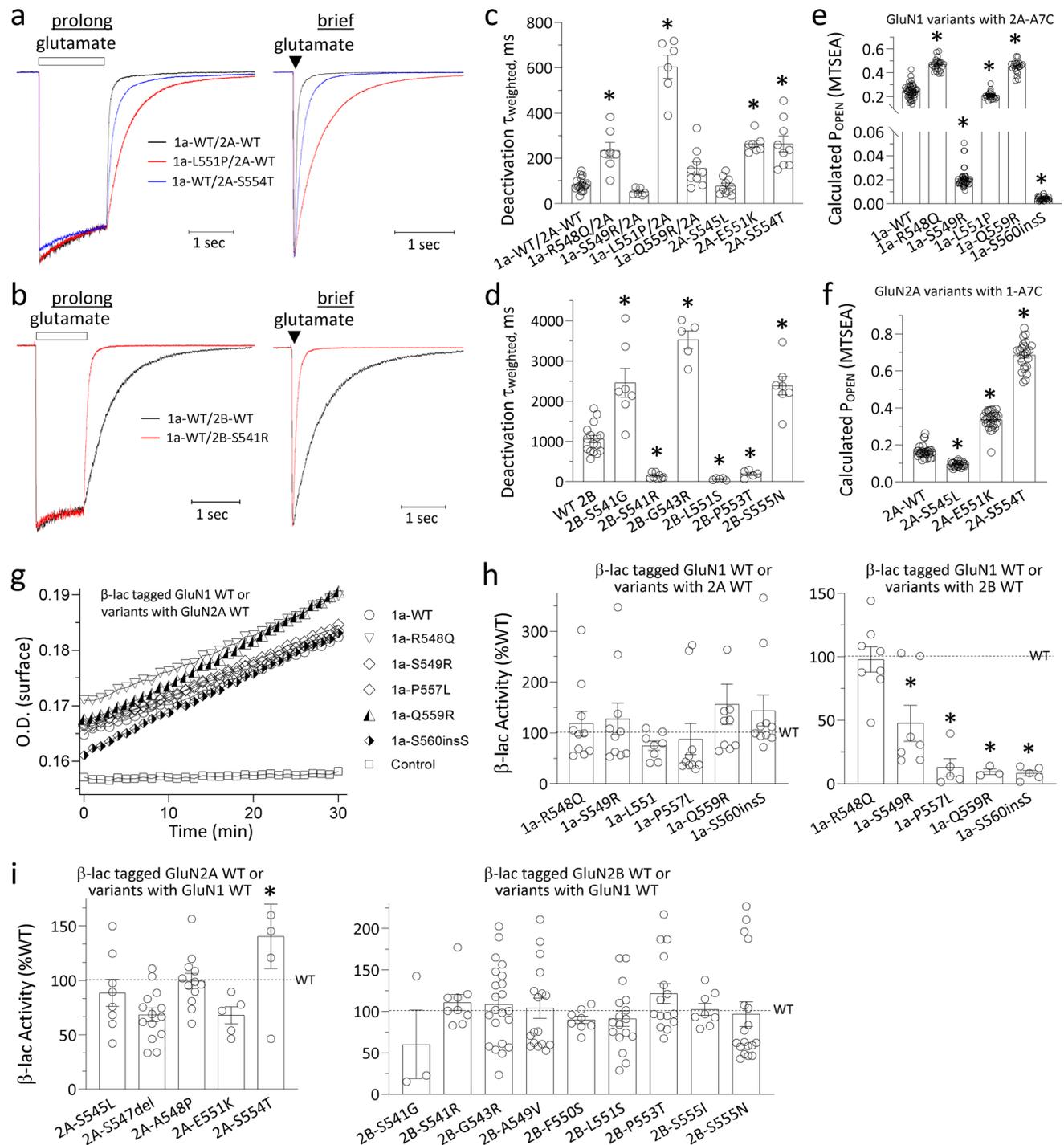
Fig. 5 Effects of pre-M1 transmembrane linker variants on NMDAR response time course and surface expression. **a** Representative recordings of the current response time course obtained from whole cell voltage clamp recordings of HEK cells transfected with WT GluN1/GluN2A (black), GluN1-L551P/GluN2A (red) and GluN1/GluN2A-S554T (blue) at a holding potential of -60 mV in response to rapid application of 1,000 μM glutamate in the presence of 100 μM glycine. *Left panel*: prolonged 1 s agonist application, *right panel*: brief 5–10 ms agonist application. **b** Representative recordings of the current response time course for the WT GluN1/GluN2B (black) and GluN1/GluN2B-S541R (red). *Left panel*: prolonged application, *right* *panel*: brief application. **c**, **d** Summary of weighted deactivation tau, *p* < 0.05, one way ANOVA with Dunnett's multiple comparisons test, compared to WT. **e**, **f** Summary of calculated channel open probability evaluated by the degree of MTSEA potentiation. **e** Representative plots of nitrocefin absorbance (optical density, O.D.) versus time are shown for HEK cells transfected with the WT β-lac-GluN1 and β-lac-GluN1variants when co-expressed with GluN2A. **g–i** Summary of the slopes of O.D. versus time were averaged as percentages of the WT NMDAR for the ratio of surface/total from 3 to 27 independent experiments. Data are presented as mean ± SEM. *p* < 0.05, one-way ANOVA with Dunnett's multiple comparisons test, compared to WT

Table 3 Response time course for pre-M1 variants

	Deactivation Tau$_{weighted}$ (ms) (n)	Steady-state/peak (%) (n)	Peak amplitude (pA/pF) (n)	P_{OPEN}, MTSEA (n)	Surface/total (% of WT) (n)
WT GluN1/2A	84 ± 6.5 (19)	70 ± 4.3 (19)	42 ± 11 (19)	0.25 ± 0.001 (48)	100 (32)
1a-R548Q/2A	236 ± 35 (7)*	76 ± 10 (7)	27 ± 13 (7)	0.47 ± 0.002 (25)*	118 ± 9.8 (10)
1a-S549R/2A	52 ± 5.9 (6)	83 ± 0.6 (6)	1.3 ± 0.3 (6)	0.02 ± 0.0002 (43)*	128 ± 9.8 (10)
1a-L551P/2A	605 ± 52 (6)*	78 ± 1.9 (6)	33 ± 16 (6)	0.21 ± 0.002 (20)*	75 ± 2.7 (9)
1a-P557L/2A	ND	ND	ND	NA	88 ± 9.6 (10)
1a-Q559R/2A	157 ± 28 (9)	80 ± 4.8 (9)	29 ± 12 (9)	0.45 ± 0.002 (28)*	156 ± 13 (10)
1a-S560insS/2A	ND	ND	ND	NA	144 ± 9.7 (10)
WT 2A				0.17 ± 0.01 (30)	100 (25)
2A-S545L	78 ± 12 (10)	65 ± 8.0 (10)	49 ± 18 (10)	0.09 ± 0.00 (25)*	89 ± 4.4 (8)
2A-S547del	ND	ND	ND	NA	68 ± 1.7 (14)
2A-A548P	ND	ND	ND	NA	100 ± 2.0 (12)
2A-E551K	264 ± 15 (7)*	79 ± 5.2 (7)	99 ± 47 (7)	0.34 ± 0.05 (30)*	68 ± 3.5 (5)
2A-S554T	264 ± 35 (9)*	50 ± 11 (9)	47 ± 22 (9)	0.69 ± 0.02 (24)*	141 ± 13 (5)*
WT 2B	1061 ± 91 (16)	74 ± 6.0 (16)	19 ± 3.6 (16)	0.026 ± 0.001 (45)	100 (87)
2B-S541G	2460 ± 362 (7)*	68 ± 10 (7)	3.7 ± 1.7 (7)*	0.045 ± 0.001 (21)*	60 ± 24 (3)
2B-S541R	142 ± 24 (8)*	89 ± 1.8 (8)	3.6 ± 1.7 (8)*	0.014 ± 0.001 (20)*	111 ± 3.2 (9)
2B-G543R	3530 ± 233 (5)*	90 ± 5.2 (5)	1.0 ± 0.4 (5)*	NA	108 ± 2.2 (22)
2B-A549V	ND	ND	ND	NA	104 ± 3.0 (17)
2B-F550S	ND	ND	ND	NA	90 ± 1.6 (8)
2B-L551S	68 ± 11 (5)*	79 ± 2.8 (5)	1.3 ± 0.7 (5)*	NA	91 ± 2.3 (17)
2B-P553T	198 ± 39 (5)*	68 ± 2.7 (5)	1.2 ± 0.5 (6)*	0.026 ± 0.001 (22)	121 ± 3.1 (15)
2B-S555I	ND	ND	ND	NA	103 ± 2.6 (8)
2B-S555N	2390 ± 229 (7)*	54 ± 4.0 (7)	8.8 ± 2.8 (7)	0.045 ± 0.001 (24)*	97 ± 3.8 (17)

Data were expressed as mean ± SEM (n), and given to 2 or 3 (e.g. Tau) significant figures. NA not available. ND not determined due to low current amplitude. % SS/peak: the ratio of peak amplitude and steady state where steady state is estimated as the current level at the end of a 1 s application of glutamate

*$p < 0.05$ one-way ANOVA, with Dunnett's multiple comparisons test, corrected family wise error by Holm Bonferroni collection

that several variants had different response amplitudes, ranging from 1 to 100 pA/pF.

Variants could also alter the probability that an agonist-bound receptor will open following full occupancy of all agonist-binding sites. To better understand the means by which variants altered the current response amplitude, we measured the open probability and biochemically determined the ratio of NMDAR protein at the cell surface to the total protein made by the cell. The effects of the pre-M1 variants on open probability were evaluated by measuring the MTSEA-induced potentiation on NMDARs that harbored a mutation in the highly conserved SYTANLAAF region of GluN1* (GluN1-A652C, hereafter 1a-A7C) and GluN2A* (GluN2A-A650C, hereafter 2A-A7C) by TEVC recording at holding potential of − 40 mV in the presence of 100 μM glutamate and 100 μM glycine [19, 33]. MTSEA modification of this Cys residue locks the channel open, and thus the degree of potentiation is inversely related to the open

probability of the receptor (see "Materials and methods"). Evaluation of open probability with this approach indicated that several variant NMDARs have significantly higher calculated open probability compared to WT, including GluN1-R548Q/GluN2A*, GluN1-Q559R/GluN2A*, GluN1*/GluN2A-E551K, GluN1*/GluN2A-S554T, GluN1*/GluN2B-S541G, and GluN1*/GluN2B-S555N (Fig. 5e, f; Table 3). However, some variants showed significantly lower calculated open probability, such as GluN1-S549R/GluN2A*, GluN1-S560insS/GluN2A*, GluN1*/GluN2A-S545L, and GluN1*/GluN2B-S541R.

Effects of pre-M1 variants on NMDAR surface expression

To evaluate whether the pre-M1 variants influence NMDAR surface expression, the cell surface protein level and total protein level were measured in transiently transfected HEK

cells. GluN1 cDNA with β-lac fused in frame to the extracellular NTD/ATD were expressed with WT or variant GluN2A or GluN2B in HEK cells. We also evaluated β-lac fused in frame to the extracellular NTD/ATD of WT GluN2A or GluN2B co-expressed with WT GluN1. The extracellularly localized β-lac will cleave the cell-impermeable chromogenic substrate nitrocefin in the extracellular solution, and the surface receptor expression can be determined using a standard enzymatic assay [18, 34]. The data (Fig. 5h) show that several GluN1 variant-containing NMDARs exhibit significantly lower surface expression compared to WT including GluN1-S549R/GluN2B (48% of WT), GluN1-P557L/GluN2B (13% of WT), GluN1-Q559A/GluN2B (10% of WT), and GluN1-Ser560insSer/GluN2B (8.3% of WT) ($p < 0.05$, one way ANOVA, with Dunnett's multiple comparisons test).

Evaluating the overall impact of pre-M1 variants on NMDA receptor function

The functional alterations induced by the disease-associated *GRIN* variants are often conflicting, as some changes can enhance current responses whereas others can reduce responses based on our in vitro assays. Therefore, we estimated the net effect of the pre-M1 variants on cellular function by combining all measured parameters to predict the alteration of synaptic and non-synaptic charge transfer mediated by the NMDAR variants compared to WT

receptors ([18, 20]; see "Materials and methods"). Our analyses indicated that GluN1-R548Q/GluN2A, GluN1-L551P/GluN2A, GluN1/GluN2A-E551K, GluN1/GluN2A-S554T, and GluN1/GluN2B-S555N showed an enhanced activity for both synaptic and non-synaptic charge transfer (Table 4), whereas GluN1-S549R/GluN2A, GluN1/GluN2B-S541R, and GluN1/GluN2B-P553T had reduced synaptic and non-synaptic charge transfer compared to WT receptors. In addition, GluN1-Q559R/GluN2A and GluN1/GluN2B-S541G had modestly enhanced activity, while GluN1/GluN2A-S545L presented a modestly reduced activity.

Discussion

In this study, we have explored the functional effects of NMDAR variants identified in the pre-M1 linker region that have been identified in affected subjects but are absent in the general population. Virtually all of the variants evaluated here altered some functional parameter or surface expression, consistent with the idea that they could contribute to the clinical phenotype. These data emphasize the important contribution of the pre-M1 linker to NMDAR gating [2–8] and are consistent with a lack of variation among healthy individuals in this region. These results clearly show that changes to the side chain of any residue in this region alters the process of channel activation.

Table 4 Summary of predicted synaptic and non-synaptic charge transfer

	Glu EC$_{50}$	Gly EC$_{50}$	Mg^{2+} IC$_{50}$	P_{OPEN}	Tau	Surface	Synaptic charge transfer	Non-synaptic charge transfer
WT GluN1/2A	–	–	–	–	–	–	1	1
1a-R548Q/2A	↑	↑	–	↑	↑	–	4.5	5.9
1a-S549R/2A	↓	↓	–	↓	↓	–	0.06	0.03
1a-L551P/2A	↑	↑	–	↓	↑	–	4.2	17
1a-Q559R/2A	↑	–	–	↑	↑	–	2.9	2.5
2A-S545L	–	↓	–	↓	–	–	0.51	0.34
2A-E551K	↑	↑	–	↑	↑	–	4.9	19
2A-S554T	↑	↑	↓	↑	↑	↑	14	43
WT GluN1/2B	–	–	–	–	–	–	1	1
2B-S541G	↑	↑	–	↑	↑	–	1.8	4.4
2B-S541R	↓	↓	↓	↓	↓	–	0.03	0.004
2B-P553T	↓	↓	–	–	↓	–	0.11	0.29
2B-S555N	↑	↑	–	↑	↑	–	4.9	15

The values of predicted synaptic and non-synaptic charge transfer changes of pre-M1 variants relative to the WT receptor (set as 1.0) were calculated by Eqs. (6), (7), and suggest the direction of potential changes synaptic and non-synaptic receptor function assuming no other compensatory mechanisms occur. ↑ A change in the indicated parameter with non-overlapping confidence intervals that should increase the response. ↓ A change in the indicated parameter with non-overlapping confidence intervals that should decrease the response. – No significant change compared to WT

Net impact of pre-M1 variants on receptor function

To better assess the actions of the pre-M1 variants, we combined the multiple functional parameters that we measured into a single indicator of whether the variant would be predicted to increase or decrease overall function both in the context of synaptic transmission (where receptors see high millimolar concentrations of glutamate for a few milliseconds) and in the context of extrasynaptic receptors, which we predict are activated by lower concentrations (0.1 μM) of ambient glutamate or glutamate released from astrocytes. Table 4 summarized the results of this analysis for eleven variants in GluN1/GluN2A and GluN1/GluN2B NMDARs (see "Materials and methods"), and shows that among the variants tested, five can be categorized as a clear gain-of-function (i.e., the variant receptor passes more synaptic and/or nonsynaptic current than WT NMDAR). Among these, GluN2A-S554T seems to show a strong increase and GluN1-R548Q and GluN1-Q559R a more modest increase in both synaptic and nonsynaptic current function, whereas GluN1-L551P (co-expressed with GluN2A), GluN2A-E551K, and GluN2B-S555N show more enhanced non-synaptic actions (Table 4). Similarly, three variants (GluN1-S549R, GluN2B-S541R, and GluN2B-P553T) show clearly reduced function both for synaptic and non-synaptic agonist levels, with GluN1-S549R and GluN2B-S541R reducing predicted currents by 16–250-fold (Table 4). These latter two variants could be considered candidates for the genetic designation loss-of-function. One variant (GluN2B-S541G) showed enhanced synaptic and non-synaptic charge transfer with more modest magnitudes and a single variant (GluN2A-S545L) had modestly reduced charge transfer, suggesting caution is warranted in classifying these variants as gain-of-function or loss-of-function.

It is also important to mention that 5 additional variants (GluN1-P557L, GluN1-S560insS, GluN2A-S547del, GluN2A-A548P) produced current levels too low in both of our heterologous expression systems to study. Therefore, these five variants are also candidates to be considered loss of function given the response amplitude is controlled by a number of factors and thus complex to interpret. For example, the overall transfection efficiency can vary from cell-to-cell, with different amounts of cDNA delivered to different cells during transfection. Moreover, cells expressing more, or fewer NMDARs might have different adherent properties, leaving a non-representative population of cells adhered to the experimental coverslip. In addition, the variants might alter the efficiency of trafficking of the receptors to the plasma membrane, and thus change the overall number of receptors that reach the membrane.

GRIN1/GluN1 pre-M1 variants

Because GluN1 serves as the obligatory subunit for all NMDARs (GluN1/GluN2A, GluN1/2B, GluN1/GluN2C, GluN1/GluN2D, GluN1/GluN3A, GluN1/GluN3B), *GRIN1* variants will impact more NMDARs than either GluN2A or GluN2B variants. For example, the gain-of-function GluN1 pre-M1 variants co-expression with GluN2B and GluN3 could be consequential early in the developing brain with the high expression levels of these three transcripts, as well as during the time after GluN2B peak expression passes and GluN2A subunit expression begins to increase throughout the CNS. NMDARs that include GluN1 pre-M1 variants that are more sensitive to glutamate and glycine could lead to increased activation at concentrations of agonists that would otherwise be too low to elicit a response. This will initiate aberrant signaling and the aberrant detection of extracellular glutamate and could lead to the overactivation of receptors whose function needs to be tightly regulated to allow for neuronal circuitry development. The gain-of-function pre-M1 variants that prolonged the deactivation time course is consistent with data for GluN1-P557R and GluN1-D552E variants [7]. Similarly, variants that diminish expression, trafficking, or function of GluN1 subunits will impact virtually all NMDA receptors in all cells, and this could have profound consequences on neuronal development and circuit function.

GRIN2A/GluN2A and GRIN2B/GluN2B pre-M1 variants

Variants in both *GRIN2A* and *GRIN2B* genes that alter amino acid sequence of the pre-M1 linker and short helix therein will potentially alter the function of any NMDARs that contain these specific subunits. Thus, GluN2B variants could have broad-ranging effects early in development, whereas GluN2A variants might alter function postnatally to adulthood of NMDARs. About half of both the GluN2A and GluN2B pre-M1 variants that we studied appear to diminish receptor function. For example, GluN2A-S547del, GluN2A-A548P, GluN2B-A549V, GluN2B-F550S, GluN2B-L551S, and GluN2B-S555I all produced currents that were too small to reliably measure in both oocytes and/or HEK cells. Interestingly, GluN2A-A548P, GluN2B-A549V, GluN2B-F550S, GluN2B-L551S, GluN2B-P553T, and GluN2B-S555I expressed at normal levels on the surface of HEK cells but gave current densities more than an order or more of magnitude lower than wild-type receptors, suggesting the diminished responses were due to deficits in gating. Several variants produced an apparent increase in function (GluN2B-S541G, GluN2B-G543R, GluN2B-S555N).

Role of pre-M1 in gating

A clear conclusion of these studies is that the pre-M1 linker and two-turn helix are key players in the sequence of events that lead to channel activation following agonist binding.

GluN1-L551P shows the strongest effects on the response time course and agonist potency. The leucine at the GluN1 position 551 has a side chain isobutyl group, making it a nonpolar aliphatic amino acid. Proline, while still considered a nonpolar aliphatic amino acid, has a side chain pyrrolidine. This cyclic structure of proline lends itself to greater conformational rigidity compared to leucine and other amino acids. As such, if the flexibility of the S1–M1 linker is required for transducing agonist binding to channel opening, then it is likely that a proline substitution in this region would disrupt this mechanism. Previously, this residue has been studied for its effects on the activity of NMDAR-positive allosteric modulator GNE-9278, which binds to the extracellular surface of the TMD. A homology model of the GluN1/GluN2A receptor puts GluN1-Leu551 near the GluN1 M1, M3, and M4 helices, as well as the GluN2A M3 helix [30]. Moreover, GluN1-Leu551 is immediately upstream of the pre-M1 helix that is involved in the gating triad consisting of the GluN1 S1–M1 linker, the GluN1 M3 helix, and the GluN2A pre-M4 helix. These three closely spaced elements control gating and multiple disease-associated mutations have been identified within these regions [2, 7, 9, 15, 35]. Moreover, modeling the effects of the GluN1-L551P variant on the position of other regions of the GluN1 subunit suggested that GluN1-L551P altered the position of the extracellular gating region of the M3 helix by 6.5 Å [30]. The requirement of the pre-M1 displacement before the M3 helix movement has been proposed [36] to prime rapid channel opening, which in turn facilitates fast synaptic signaling.

Role of pre-M1 variants in neurological disease

GRIN variants have been identified in patients displaying a wide range of clinical features, including (but not limited to) intellectual disability, developmental delay, epilepsy, movement disorders, and language and speech issues [1, 37, 38]. Any aberrant NMDAR activation profile in developing CNS tissue that produces too little or too much NMDAR function will almost certainly trigger compensatory mechanisms and could alter NMDAR-developmental programs that impact entire populations of neurons [39–42]. In addition, persistent aberrant receptor function could alter circuit function or synaptic plasticity in a manner that produces clinical symptoms in its own right. Thus, there are two potential consequences of variation (compensation, altered receptor function) driving changes in brain function that manifest as clinical symptoms. Furthermore, enhanced currents produced by variant NMDARs in some cases could elevate levels of Ca^{2+} influx that trigger dendritic, axonal, or neuronal damage secondary to excitotoxic processes [43, 44]. NMDAR hyperfunction has also been suggested to be linked to multiple neurological disorders including Alzheimer's disease [45], Huntington's disease [46], epilepsy [37]. Thus, it is possible that variants that lead to increased charge transfer could engage some underlying features of these disorders.

NMDAR hypofunction has been associated with schizophrenia [47, 48] and memory impairment [48]. It seems possible that the loss-of-function pre-M1 variants evaluated in this study (i.e., GluN1-S549R/GluN2A, GluN1/2A-S545L) may lead to overall hypofunction of the NMDARs by reducing agonist potency, shortening response time course, decreasing channel open probability, and/or reducing surface expression. These variants could drive pathological circuit function by altering the balance of excitatory and inhibitory inputs in CNS or dramatically changing the overall charge transfer of a synaptic or non-synaptic receptor.

One clear result from multiple mouse models of *GRIN* variants is that the features observed in heterologous receptors can be manifest in some neurons [49–51], however, the neuronal context and subunit composition of variant-containing receptors can alter the extent to which specific functional changes appear.

Declarations

References

1. Hansen KB, Wollmuth LP, Bowie D, Furukawa H, Menniti FS, Sobolevsky AI, Swanson GT, Swanger SA, Greger IH, Nakagawa T, McBain CJ, Jayaraman V, Low CM, Dell'Acqua ML, Diamond JS, Camp CR, Perszyk RE, Yuan HJ, Traynelis SF (2021) Structure, function, and pharmacology of glutamate receptor ion channels. Pharmacol Rev 73(4):298–487. https://doi.org/10.1124/pharmrev.120.000131

2. Perszyk RE, Myers SJ, Yuan H, Gibb AJ, Furukawa H, Sobolevsky AI, Traynelis SF (2020) Hodgkin–Huxley–Katz Prize Lecture: genetic and pharmacological control of glutamate receptor channel through a highly conserved gating motif. J Physiol. https://doi.org/10.1113/JP278086

3. Talukder I, Borker P, Wollmuth LP (2010) Specific sites within the ligand-binding domain and ion channel linkers modulate NMDA receptor gating. J Neurosci 30(35):11792–11804. https://doi.org/10.1523/Jneurosci.5382-09.2010

4. Sobolevsky AI, Rosconi MP, Gouaux E (2009) X-ray structure, symmetry and mechanism of an AMPA-subtype glutamate receptor. Nature 462(7274):745–756. https://doi.org/10.1038/nature08624

5. Karakas E, Furukawa H (2014) Crystal structure of a heterotetrameric NMDA receptor ion channel. Science 344(6187):992–997. https://doi.org/10.1126/science.1251915

6. Lee CH, Lu W, Michel JC, Goehring A, Du J, Song X, Gouaux E (2014) NMDA receptor structures reveal subunit arrangement and pore architecture. Nature 511(7508):191–197. https://doi.org/10.1038/nature13548

7. Ogden KK, Chen W, Swanger SA, McDaniel MJ, Fan LZ, Hu C, Tankovic A, Kusumoto H, Kosobucki GJ, Schulien AJ, Su Z, Pecha J, Bhattacharya S, Petrovski S, Cohen AE, Aizenman E, Traynelis SF, Yuan H (2017) Molecular mechanism of disease-associated mutations in the pre-M1 helix of NMDA receptors and potential rescue pharmacology. PLoS Genet 13(1):e1006536. https://doi.org/10.1371/journal.pgen.1006536

8. Gibb AJ, Ogden KK, McDaniel MJ, Vance KM, Kell SA, Butch C, Burger P, Liotta DC, Traynelis SF (2018) A structurally derived model of subunit-dependent NMDA receptor function. J Physiol 596(17):4057–4089. https://doi.org/10.1113/JP276093

9. Amin JB, Moody GR, Wollmuth LP (2020) From bedside-to-bench: what disease-associated variants are teaching us about the NMDA receptor. J Physiol. https://doi.org/10.1113/JP278705

10. Soto D, Olivella M, Grau C, Armstrong J, Alcon C, Gasull X, Santos-Gomez A, Locubiche S, Gomez de Salazar M, Garcia-Diaz R, Gratacos-Batlle E, Ramos-Vicente D, Chu-Van E, Colsch B, Fernandez-Duenas V, Ciruela F, Bayes A, Sindreu C, Lopez-Sala A, Garcia-Cazorla A, Altafaj X (2019) L-Serine dietary supplementation is associated with clinical improvement of loss-of-function GRIN2B-related pediatric encephalopathy. Sci Signal. https://doi.org/10.1126/scisignal.aaw0936

11. Perszyk RE, Kristensen AS, Lyuboslavsky P, Traynelis SF (2021) Three-dimensional missense tolerance ratio analysis. Genome Res 31(8):1447–1461. https://doi.org/10.1101/gr.275528.121

12. Chou TH, Tajima N, Romero-Hernandez A, Furukawa H (2020) Structural basis of functional transitions in mammalian NMDA receptors. Cell 182(2):357-371.e13. https://doi.org/10.1016/j.cell.2020.05.052

13. Hedegaard M, Hansen KB, Andersen KT, Brauner-Osborne H, Traynelis SF (2012) Molecular pharmacology of human NMDA receptors. Neurochem Int 61(4):601–609. https://doi.org/10.1016/j.neuint.2011.11.016

14. Yuan H, Hansen KB, Zhang J, Pierson TM, Markello TC, Fajardo KV, Holloman CM, Golas G, Adams DR, Boerkoel CF, Gahl WA, Traynelis SF (2014) Functional analysis of a de novo GRIN2A missense mutation associated with early-onset epileptic encephalopathy. Nat Commun 5:3251. https://doi.org/10.1038/ncomms4251

15. Chen W, Tankovic A, Burger PB, Kusumoto H, Traynelis SF, Yuan H (2017) Functional evaluation of a de novo GRIN2A mutation identified in a patient with profound global developmental delay and refractory epilepsy. Mol Pharmacol 91(4):317–330. https://doi.org/10.1124/mol.116.106781

16. XiangWei W, Kannan V, Xu Y, Kosobucki GJ, Schulien AJ, Kusumoto H, Moufawad El Achkar C, Bhattacharya S, Lesca G, Nguyen S, Helbig KL, Cuisset JM, Fenger CD, Marjanovic D, Schuler E, Wu Y, Bao X, Zhang Y, Dirkx N, Schoonjans AS, Syrbe S, Myers SJ, Poduri A, Aizenman E, Traynelis SF, Lemke JR, Yuan H, Jiang Y (2019) Heterogeneous clinical and functional features of GRIN2D-related developmental and epileptic encephalopathy. Brain 142(10):3009–3027. https://doi.org/10.1093/brain/awz232

17. Erreger K, Traynelis SF (2008) Zinc inhibition of rat NR1/NR2A N-methyl-D-aspartate receptors. J Physiol-London 586(3):763–778. https://doi.org/10.1113/jphysiol.2007.143941

18. Swanger SA, Chen W, Wells G, Burger PB, Tankovic A, Bhattacharya S, Strong KL, Hu C, Kusumoto H, Zhang J, Adams DR, Millichap JJ, Petrovski S, Traynelis SF, Yuan H (2016) Mechanistic insight into NMDA receptor dysregulation by rare variants in the GluN2A and GluN2B agonist binding domains. Am J Hum Genet 99(6):1261–1280. https://doi.org/10.1016/j.ajhg.2016.10.002

19. Yuan H, Erreger K, Dravid SM, Traynelis SF (2005) Conserved structural and functional control of N-methyl-D-aspartate receptor gating by transmembrane domain M3. J Biol Chem 280(33):29708–29716. https://doi.org/10.1074/jbc.M414215200

20. Li J, Zhang J, Tang W, Mizu RK, Kusumoto H, XiangWei W, Xu Y, Chen W, Amin JB, Hu C, Kannan V, Keller SR, Wilcox WR, Lemke JR, Myers SJ, Swanger SA, Wollmuth LP, Petrovski S, Traynelis SF, Yuan H (2019) De novo GRIN variants in NMDA receptor M2 channel pore-forming loop are associated with neurological diseases. Hum Mutat 40(12):2393–2413. https://doi.org/10.1002/humu.23895

21. Hamdan FF, Gauthier J, Araki Y, Lin DT, Yoshizawa Y, Higashi K, Park AR, Spiegelman D, Dobrzeniecka S, Piton A, Tomitori H, Daoud H, Massicotte C, Henrion E, Diallo O, Group SD, Shekarabi M, Marineau C, Shevell M, Maranda B, Mitchell G, Nadeau A, D'Anjou G, Vanasse M, Srour M, Lafreniere RG, Drapeau P, Lacaille JC, Kim E, Lee JR, Igarashi K, Huganir RL, Rouleau GA, Michaud JL (2011) Excess of de novo deleterious mutations in genes associated with glutamatergic systems in nonsyndromic intellectual disability. Am J Hum Genet 88(3):306–316. https://doi.org/10.1016/j.ajhg.2011.02.001

22. Lemke JR, Lal D, Reinthaler EM, Steiner I, Nothnagel M, Alber M, Geider K, Laube B, Schwake M, Finsterwalder K, Franke A, Schilhabel M, Jahn JA, Muhle H, Boor R, Van Paesschen W, Caraballo R, Fejerman N, Weckhuysen S, De Jonghe P, Larsen J, Moller RS, Hjalgrim H, Addis L, Tang S, Hughes E, Pal DK, Veri K, Vaher U, Talvik T, Dimova P, Guerrero Lopez R, Serratosa JM, Linnankivi T, Lehesjoki AE, Ruf S, Wolff M, Buerki S, Wohlrab G, Kroell J, Datta AN, Fiedler B, Kurlemann G, Kluger G, Hahn A, Haberlandt DE, Kutzer C, Sperner J, Becker F, Weber YG, Feucht M, Steinbock H, Neophythou B, Ronen GM, Gruber-Sedlmayr U, Geldner J, Harvey RJ, Hoffmann P, Herms S, Altmuller J, Toliat MR, Thiele H, Nurnberg P, Wilhelm C, Stephani U, Helbig I, Lerche H, Zimprich F, Neubauer BA, Biskup S, von Spiczak S (2013) Mutations in GRIN2A cause idiopathic focal epilepsy with rolandic spikes. Nat Genet 45(9):1067–1072. https://doi.org/10.1038/ng.2728

23. Redin C, Gerard B, Lauer J, Herenger Y, Muller J, Quartier A, Masurel-Paulet A, Willems M, Lesca G, El-Chehadeh S, Le Gras S, Vicaire S, Philipps M, Dumas M, Geoffroy V, Feger C, Haumesser N, Alembik Y, Barth M, Bonneau D, Colin E, Dollfus H, Doray B, Delrue MA, Drouin-Garraud V, Flori E, Fradin M, Francannet C, Goldenberg A, Lumbroso S, Mathieu-Dramard M, Martin-Coignard D, Lacombe D, Morin G, Polge A, Sukno S, Thauvin-Robinet C, Thevenon J, Doco-Fenzy M, Genevieve D, Sarda P, Edery P, Isidor B, Jost B, Olivier-Faivre L, Mandel JL, Piton A (2014) Efficient strategy for the molecular diagnosis of intellectual disability using targeted high-throughput sequencing. J Med Genet 51(11):724–736. https://doi.org/10.1136/jmedgenet-2014-102554

24. Helbig K, Hagman KF, Powis Z, Tang S, Helbig I (2016) Whole exome sequencing in the epilepsies: the developing diagnostic exome signature of epilepsy genes over a 5-year period. Epilepsia 57:29–29

25. Lemke JR, Geider K, Helbig KL, Heyne HO, Schutz H, Hentschel J, Courage C, Depienne C, Nava C, Heron D, Moller RS, Hjalgrim H, Lal D, Neubauer BA, Nurnberg P, Thiele H, Kurlemann G, Arnold GL, Bhambhani V, Bartholdi D, Pedurupillay CRJ, Misceo D, Frengen E, Stromme P, Dlugos DJ, Doherty ES, Bijlsma EK, Ruivenkamp CA, Hoffer MJV, Goldstein A, Rajan DS, Narayanan V, Ramsey K, Belnap N, Schrauwen I, Richholt R, Koeleman BPC, Sa J, Mendonca C, de Kovel CGF, Weckhuysen S, Hardies K, De Jonghe P, De Meirleir L, Milh M, Badens C, Lebrun M, Busa T, Francannet C, Piton A, Riesch E, Biskup S, Vogt H, Dorn T, Helbig I, Michaud JL, Laube B, Syrbe S (2016) Delineating the GRIN1 phenotypic spectrum: a distinct genetic NMDA receptor encephalopathy. Neurology 86(23):2171–2178. https://doi.org/10.1212/Wnl.0000000000002740

26. Lucariello M, Vidal E, Vidal S, Saez M, Roa L, Huertas D, Pineda M, Dalfo E, Dopazo J, Jurado P, Armstrong J, Esteller M (2016) Whole exome sequencing of Rett syndrome-like patients reveals the mutational diversity of the clinical phenotype. Hum Genet 135(12):1343–1354. https://doi.org/10.1007/s00439-016-1721-3

27. Retterer K, Juusola J, Cho MT, Vitazka P, Millan F, Gibellini F, Vertino-Bell A, Smaoui N, Neidich J, Monaghan KG, McKnight D, Bai RK, Suchy S, Friedman B, Tahiliani J, Pineda-Alvarez D, Richard G, Brandt T, Haverfield E, Chung WK, Bale S (2016) Clinical application of whole-exome sequencing across clinical indications. Genet Med 18(7):696–704. https://doi.org/10.1038/gim.2015.148

28. Platzer K, Yuan H, Schutz H, Winschel A, Chen W, Hu C, Kusumoto H, Heyne HO, Helbig KL, Tang S, Willing MC, Tinkle BT, Adams DJ, Depienne C, Keren B, Mignot C, Frengen E, Stromme P, Biskup S, Docker D, Strom TM, Mefford HC, Myers CT, Muir AM, LaCroix A, Sadleir L, Scheffer IE, Brilstra E, van Haelst MM, van der Smagt JJ, Bok LA, Moller RS, Jensen UB, Millichap JJ, Berg AT, Goldberg EM, De Bie I, Fox S, Major P, Jones JR, Zackai EH, Abou Jamra R, Rolfs A, Leventer RJ, Lawson JA, Roscioli T, Jansen FE, Ranza E, Korff CM, Lehesjoki AE, Courage C, Linnankivi T, Smith DR, Stanley C, Mintz M, McKnight D, Decker A, Tan WH, Tarnopolsky MA, Brady LI, Wolff M, Dondit L, Pedro HF, Parisotto SE, Jones KL, Patel AD, Franz DN, Vanzo R, Marco E, Ranells JD, Di Donato N, Dobyns WB, Laube B, Traynelis SF, Lemke JR (2017) GRIN2B encephalopathy: novel findings on phenotype, variant clustering, functional consequences and treatment aspects. J Med Genet 54(7):460–470. https://doi.org/10.1136/jmedgenet-2016-104509

29. Tan TY, Dillon OJ, Stark Z, Schofield D, Alam K, Shrestha R, Chong B, Phelan D, Brett GR, Creed E, Jarmolowicz A, Yap P, Walsh M, Downie L, Amor DJ, Savarirayan R, McGillivray G, Yeung A, Peters H, Robertson SJ, Robinson AJ, Macciocca I, Sadedin S, Bell K, Oshlack A, Georgeson P, Thorne N, Gaff C, White SM (2017) Diagnostic impact and cost-effectiveness of whole-exome sequencing for ambulant children with suspected monogenic conditions. Jama Pediatr 171(9):855–862. https://doi.org/10.1001/jamapediatrics.2017.1755

30. Fry AE, Fawcett KA, Zelnik N, Yuan HJ, Thompson BAN, Shemer-Meiri L, Cushion TD, Mugalaasi H, Sims D, Stoodley N, Chung SK, Rees MI, Patel CV, Brueton LA, Layet V, Giuliano F, Kerr MP, Banne E, Meiner V, Lerman-Sagie T, Helbig KL, Kofman LH, Knight KM, Chen WJ, Kannan V, Hu C, Kusumoto H, Zhang J, Swanger SA, Shaulsky GH, Mirzaa GM, Muir AM, Mefford HC, Dobyns WB, Mackenzie AB, Mullins JGL, Lemke JR, Bahi-Buisson N, Traynelis SF, Iago HF, Pilz DT (2018) De novo mutations in GRIN1 cause extensive bilateral polymicrogyria. Brain 141:698–712. https://doi.org/10.1093/brain/awx358

31. Stanek D, Lassuthova P, Sterbova K, Vlckova M, Neupauerova J, Krutova M, Seeman P (2018) Detection rate of causal variants in severe childhood epilepsy is highest in patients with seizure onset within the first four weeks of life. Orphanet J Rare Dis 13:71. https://doi.org/10.1186/s13023-018-0812-8

32. Frisk S, Wachtmeister A, Laurell T, Lindstrand A, Jantti N, Malmgren H, Lagerstedt-Robinson K, Tesi B, Taylan F, Nordgren A (2022) Detection of germline mosaicism in fathers of children with intellectual disability syndromes caused by de novo variants. Mol Genet Genom Med 10(4):e1880. https://doi.org/10.1002/mgg3.1880

33. Jones KS, VanDongen HM, VanDongen AM (2002) The NMDA receptor M3 segment is a conserved transduction element coupling ligand binding to channel opening. J Neurosci 22(6):2044–2053

34. Lam VM, Beerepoot P, Angers S, Salahpour A (2013) A novel assay for measurement of membrane-protein surface expression using a beta-lactamase reporter. Traffic 14(7):778–784. https://doi.org/10.1111/tra.12073

35. McDaniel MJ, Ogden KK, Kell SA, Burger PB, Liotta DC, Traynelis SF (2020) NMDA receptor channel gating control by the pre-M1 helix. J Gen Physiol 152(4):e201912362. https://doi.org/10.1085/jgp.201912362

36. Amin JB, Gochman A, He M, Certain N, Wollmuth LP (2021) NMDA receptors require multiple pre-opening gating steps for efficient synaptic activity. Neuron 109:488-501.e4. https://doi.org/10.1016/j.neuron.2020.11.009

37. XiangWei W, Jiang Y, Yuan H (2018) De novo mutations and rare variants occurring in NMDA receptors. Curr Opin Physiol 2:27–35. https://doi.org/10.1016/j.cophys.2017.12.013

38. Strehlow V, Heyne HO, Vlaskamp DRM, Marwick KFM, Rudolf G, de Bellescize J, Biskup S, Brilstra EH, Brouwer OF, Callenbach PMC, Hentschel J, Hirsch E, Kind PC, Mignot C, Platzer K, Rump P, Skehel PA, Wyllie DJA, Hardingham GE, van Ravenswaaij-Arts CMA, Lesca G, Lemke JR, group GAs (2019) GRIN2A-related disorders: genotype and functional consequence

predict phenotype. Brain 142(1):80–92. https://doi.org/10.1093/brain/awy304

39. Matta JA, Pelkey KA, Craig MT, Chittajallu R, Jeffries BW, McBain CJ (2013) Developmental origin dictates interneuron AMPA and NMDA receptor subunit composition and plasticity. Nat Neurosci 16(8):1032-U1087. https://doi.org/10.1038/nn.3459

40. Kannangara TS, Bostrom CA, Ratzlaff A, Thompson L, Cater RM, Gil-Mohapel J, Christie BR (2014) Deletion of the NMDA receptor GluN2A subunit significantly decreases dendritic growth in maturing dentate granule neurons. PLoS ONE 9(8):e103155. https://doi.org/10.1371/journal.pone.0103155

41. Perszyk RE, DiRaddo JO, Strong KL, Low CM, Ogden KK, Khatri A, Vargish GA, Pelkey KA, Tricoire L, Liotta DC, Smith Y, McBain CJ, Traynelis SF (2016) GluN2D-containing N-methyl-D-aspartate receptors mediate synaptic transmission in hippocampal interneurons and regulate interneuron activity. Mol Pharmacol 90(6):689–702. https://doi.org/10.1124/mol.116.105130

42. Booker SA, Sumera A, Kind PC, Wyllie DJA (2021) Contribution of NMDA receptors to synaptic function in rat hippocampal interneurons. Eneuro. https://doi.org/10.1523/Eneuro.0552-20.2021. (**Artn 0552-20.2021**)

43. Choi DW (1992) Excitotoxic cell-death. J Neurobiol 23(9):1261–1276. https://doi.org/10.1002/neu.480230915

44. Choi DW (1994) Calcium and excitotoxic neuronal injury. Ann Ny Acad Sci 747:162–171

45. Hynd MR, Scott HL, Dodd PR (2004) NMDA receptor dysfunction in Alzheimer's disease. J Neurochem 88:50–50

46. Zeron MM, Hansson O, Chen NS, Wellington CL, Leavitt BR, Brundin P, Hayden MR, Raymond LA (2002) Increased sensitivity to N-methyl-D-aspartate receptor-mediated excitotoxicity in a mouse model of Huntington's disease. Neuron 33(6):849–860. https://doi.org/10.1016/S0896-6273(02)00615-3

47. Coyle JT (2006) Substance use disorders and schizophrenia: a question of shared glutamatergic mechanisms. Neurotox Res 10(3–4):221–233. https://doi.org/10.1007/Bf03033359

48. Olney JW, Newcomer JW, Farber NB (1999) NMDA receptor hypofunction model of schizophrenia. J Psychiat Res 33(6):523–533. https://doi.org/10.1016/S0022-3956(99)00029-1

49. Amador A, Bostick CD, Olson H, Peters J, Camp CR, Krizay D, Chen W, Han W, Tang W, Kanber A, Kim S, Teoh J, Sah M, Petri S, Paek H, Kim A, Lutz CM, Yang M, Myers SJ, Bhattacharya S, Yuan H, Goldstein DB, Poduri A, Boland MJ, Traynelis SF, Frankel WN (2020) Modelling and treating GRIN2A developmental and epileptic encephalopathy in mice. Brain 143(7):2039–2057. https://doi.org/10.1093/brain/awaa147

50. Shin W, Kim K, Serraz B, Cho YS, Kim D, Kang M, Lee EJ, Lee H, Bae YC, Paoletti P, Kim E (2020) Early correction of synaptic long-term depression improves abnormal anxiety-like behavior in adult GluN2B-C456Y-mutant mice. PLoS Biol 18(4):e3000717. https://doi.org/10.1371/journal.pbio.3000717

51. Bertocchi I, Eltokhi A, Rozov A, Chi VN, Jensen V, Bus T, Pawlak V, Serafino M, Sonntag H, Yang B, Burnashev N, Li SB, Obenhaus HA, Both M, Niewoehner B, Single FN, Briese M, Boerner T, Gass P, Rawlins JNP, Kohr G, Bannerman DM, Sprengel R (2021) Voltage-independent GluN2A-type NMDA receptor Ca(2+) signaling promotes audiogenic seizures, attentional and cognitive deficits in mice. Commun Biol 4(1):59. https://doi.org/10.1038/s42003-020-01538-4

52. Han W, Yuan H, Allen JP, Kim S, Shaulsky GH, Perszyk RE, Traynelis SF, Myers SJ (2022) Opportunities for precision treatment of GRIN2A and GRIN2B gain-of-function variants in triheteromeric N-methyl-D-aspartate receptors. J Pharmacol Exp Ther 381(1):54–66. https://doi.org/10.1124/jpet.121.001000